SOLAR CONCENTRATION BY CURVED-BASE FRESNEL LENSES

Ronald M. Cosby

1. REPORT NO. NASA CR-2890	2. GOVERNMENT ACCESSION NO.	3. RECIPIENT'S CATALOG NO.
4. TITLE AND SUBTITLE Solar Concentration by Curved-Base Fresnel Lenses		5. REPORT DATE August 1977
		6. PERFORMING ORGANIZATION CODE
7. AUTHOR(S) Ronald M. Cosby		8. PERFORMING ORGANIZATION REPORT # M-229
9. PERFORMING ORGANIZATION NAME AND ADDRESS Department of Physics and Astronomy Ball State University Muncie, Indiana		10. WORK UNIT NO.
		11. CONTRACT OR GRANT NO. NCA8-00127, Mod 4
12. SPONSORING AGENCY NAME AND ADDRESS National Aeronautics and Space Administration Washington, D. C. 20546		13. TYPE OF REPORT & PERIOD COVERED Contractor Report
		14. SPONSORING AGENCY CODE

15. SUPPLEMENTARY NOTES

16. ABSTRACT

The solar concentration performance of idealized curved-base line-focusing Fresnel lenses is analyzed in this report. A simple optical model is introduced to study the effects of base curvature and lens f-number. Thin lens ray tracing and the laws of reflection and refraction are used to develop expressions for lens transmittance and image plane intensity profiles. The intensity distribution over the solar spectrum, lens dispersion effects, and absorption by the lens material are included in the analysis. Model capabilities include assessment of lens performance in the presence of small transverse tracking errors and the sensitivity of solar image characteristics to defocusing.

Computer-generated example data for a lens with a 36 inch (91.4 cm) wide aperture indicate substantial improvements in solar optical performance over the flat Fresnel lens occur when base curvature is introduced. The primary measure of lens performance is the width of a target receptor centrally located in an image plane that is required to intercept a given constant fraction of the incident sunlight on the concentrator. The image profile shapes, positions, and peak concentration ratios are discussed in addition to lens transmission details.

(Abstract continued on reverse side.)

17. KEY WORDS	18. DISTRIBUTION STATEMENT Unclassified - Unlimited STAR CAT. 74
19. SECURITY CLASSIF. (of this report) Unclassified	20. SECURITY CLASSIF. (of this page) Unclassified	21. NO. OF PAGES 66	22. PRICE $4.50

Abstract (continued)

Solar concentration characteristics are studied for lenses with f-numbers from 0.7 to 1.0 and curvatures ranging from the flat lens case to the minimum possible radius of curvature. For selected lenses, the effects of small transverse tracking errors (0°-2°) and slight defocusing (±2% of the focal length) are investigated and compared to flat lens performance sensitivities.

Curving the lens base significantly reduces required target widths. Lens solar transmission is generally in the range 85-88% with mild dependence on curvature. Transverse tracking error sensitivities are substantially improved by curving the lens base. The principle negative effect of curvature is a considerable increase in the rate of degradation of image profile characteristics with slight defocusing. Optimum radii of curvature for ideal lens solar concentrators are generally found near the minimum possible values.

In comparison to an f/1.0 flat lens, selection of a curved base Fresnel lens with $0.8 \leq$ f-number < 1.0 and curvature radius $R \leq$ focal length is predicted to improve the solar optical performance while decreasing support structure and tracking system requirements.

TABLE OF CONTENTS

LIST OF ILLUSTRATIONS

LIST OF ILLUSTRATIONS (Cont.)

LIST OF TABLES

vi

SYMBOL	DEFINITION
A	total lens sunlight transmittance
A_j	lens transmittance for the jth spectral interval
d	defocus length parameter
f	lens focal length
$I_{ij}(Y)$	intensity contribution from ith serration and jth spectral interval
$I_i(Y)$	ith serration sunlight intensity contribution at position Y
$I_j(Y)$	intensity at position Y from solar flux in jth spectral interval
$I(Y)$	total intensity at position Y
i	serration index
j	spectral index
L, L_{ij}	beam spread for sunlight within jth spectral interval refracted by ith serration
N	design index of refraction
n	index of refraction
q	incident solar intensity (direct sunlight only)
q_j	incident solar intensity in jth spectral interval
R	lens radius of curvature
s	serration arc position
Δs	serration arc width
T_a	bulk transmittance factor
T_1, T_2	Fresnel transmittance factors for smooth and serrated lens surfaces, respectively
T, T_{ij}	transmittance for ith serration for sunlight in jth spectral interval

SYMBOL	DEFINITION
T_i	serration sunlight transmittance
W	lens aperture width
(x_t, y_t) (x_b, y_b)	serration edge coordinates
(x_b', y_b') (x_b'', y_b'')	extreme ray serration exit coordinates
y	distance from lens centerline and normal to the optic axis
Y	position variable in image plane
$Y1, Y2, Y3, Y4$	extreme ray intercepts
2α	apparent angular diameter of Sun
β_t, β_b	serration edge angular coordinates
γ	extreme ray emergence angle for solar design wavelength
$\gamma_b, \gamma_t, \gamma_b', \gamma_t'$	extreme ray emergence angles
δ	transverse tracking error
θ	groove angle with respect to lens surface
θ_v	complement of groove angle with respect to optic axis
$\Delta\lambda_j$	jth wavelength interval
ϕ	serration angular coordinate
$\phi_{inc}, \phi', \phi_i$	angles of incidence
$\phi_{ref}, \phi_t', \phi_t, \phi_b, \phi_b'$	angles of refraction
ω_j	solar spectral weighting factor

I. INTRODUCTION

Fresnel lens solar concentrators offer potentially economical alternatives to mirror focusing devices. The solar concentration performance of one such concentrator, the flat, line-focusing Fresnel lens, has recently been investigated analytically and experimentally [1-5]. Possible improvement in the solar optical performance of this type of concentrator is suggested if the smooth base surface is curved rather than flat. This curvature introduces a second optically active surface for the refraction and redirection of incident sunlight.

This report presents a simple analytical model for determining the solar concentration characteristics of a tracking, curved-base, line-focusing Fresnel lens (Figure 1) and displays example data to demonstrate overall performance sensitivities. The thin lens analytical model uses ray tracing and empirical procedures similar to those introduced in earlier descriptions of the flat lens [3-5]. Lens solar transmission and imaging properties are evaluated for a variety of lens parameters and optical conditions.

Reducing the f-number of a lens concentrator is desirable for lowering structural support and tracking mechanism sizes and costs. For flat lenses, such reductions degrade the solar optical performance of the concentrator. One objective of the present study is to examine the solar concentration characteristics of curved lenses with f-numbers less than one.

A second objective is to determine the overall effects of curvature on lens performance. If an optimum lens curvature exists, identification of that curvature is desired.

SUNLIGHT

LINE
IMAGE
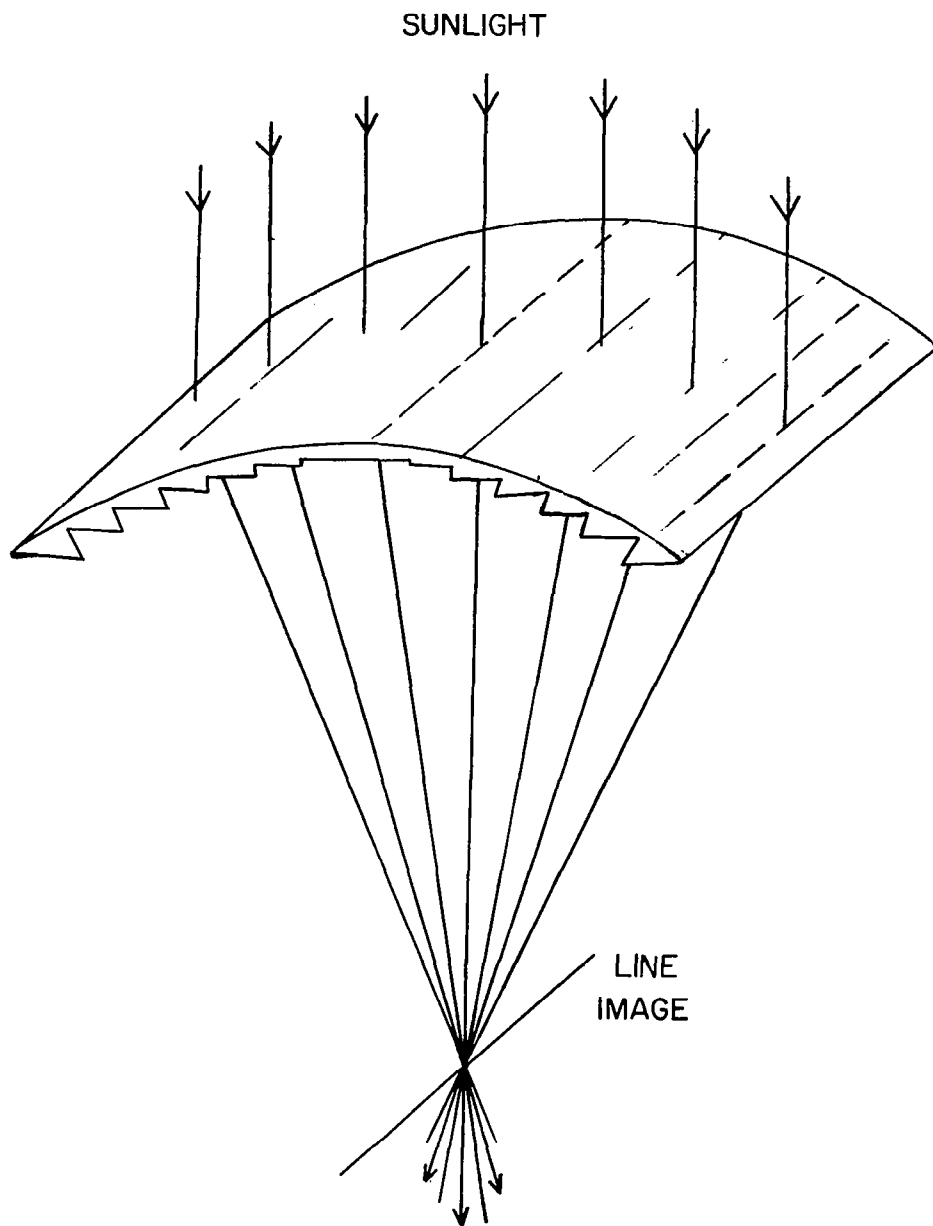
Figure 1. Curved-base Fresnel lens solar concentrator.

Attainment of the above goals requires investigation of the lens transmittance and imaging characteristics in the presence of tracking errors. An appraisal of curved lens performance sensitivity to small transverse tracking errors is therefore one aim of this analysis. Longitudinal (axial) tracking errors are not dealt with in the simple optical model. However, experience with flat test lenses has shown little change in concentration properties for small longitudinal errors [1,4,5].

The sensitivity of solar image characteristics to slight defocusing is important in the consideration of the design and placement of target receptors. Inclusion of this aspect of lens performance in evaluating curved lens solar concentrators is also an objective of the present work.

To aid in understanding lens performance as related to the above goals, the curved lens analytical model is applied to an example lens using a computer program for data generation and display.

II. CURVED LENS ANALYTICAL MODEL

Modelling the solar concentration performance of a Fresnel lens presents a different and in some ways simpler problem than the usual optical problem of analyzing lens aberrations and image defects. The primary objective of a solar concentrator is the maximum transmission, concentration, and localization of solar energy. Solar image clarity and image defects are important only as they affect the realization of this primary objective. Therefore, the analytical model presented here deals with lens transmission and the distribution of concentrated energy in selected planes beneath the lens and normal to the optic axis. Differences between the present model and earlier flat lens analyses [3-5] arise only as a result of changes in lens geometry.

Simple ray optics and the laws of reflection and refraction are used to develop theoretical expressions for lens transmittance and image intensity. The solar spectral intensity distribution and dispersion effects are included. Both surface reflection losses and bulk absorption affect lens transmission in this model. To facilitate evaluation of major lens performance sensitivities, a number of simplifying assumptions have been made. A discussion of these assumptions is followed by analyses of required groove angles, lens transmission characteristics, and image intensity profiles for a curved lens solar concentrator.

A. Model Assumptions

The ray trace model assumes a grooves down, thin, curved-base, line-focusing Fresnel lens. The thin lens assumption simplifies the necessary ray tracing for computing groove angles, serration transmission coefficients, and image plane extreme ray intercepts. Manufacturing defects, wind loading, and thermal expansion effects are not considered. Other model assumptions include:

1. Lens orientation in the seasonal (longitudinal or axial) direction is perfect.

2. The solar flux refracted by a single serration is (a) bounded by the refracted extreme rays from the edge of the solar disc that have zero axial ray components, and (b) uniformly distributed over the beam spread width in the intercept plane beneath the lens.

3. The Sun is a uniform radiation source, i.e., all points on the solar disc are assumed to have equal energy emission rates.

4. Diffraction effects are negligible and no anomalous dispersion effects near absorption bands in the lens material occur.

The assumed groove geometry places serrations on a curved surface such that the serration edge is normal to the lens base arc.

4

B. Groove Angles

The groove angles required for perfect focusing of incident parallel light of a chosen design wavelength can be determined using Snell's law of refraction and simple geometrical relations. Referring to the ray diagrams in Figure 2 and using Snell's law at each lens surface,

$$\sin \phi = N \sin \phi_t \qquad (1)$$

and

$$N \sin \phi' = \sin \phi_t' , \qquad (2)$$

where

$$\phi' = \phi - \phi_t + \theta_v , \qquad (3)$$

$$\phi_t' = \gamma + \theta_v , \qquad (4)$$

and N is the design refractive index. Using Equations (2) thru (4),

$$\tan \theta_v = \frac{N \sin (\phi - \phi_t) - \sin \gamma}{\cos \gamma - N \cos (\phi - \phi_t)} \qquad (5)$$

where from Equation (1),

$$\phi_t = \text{Arcsin} \left(\frac{\sin \phi}{N}\right) . \qquad (6)$$

Assuming a thin lens base and diminutive serration height,

$$\tan \gamma \simeq \frac{y}{f - R + \sqrt{R^2 - y^2}} \qquad (7)$$

where y is the center position of the serration relative to the lens optic axis, R the curvature radius, and f the lens focal length. Now

$$y = R \sin \phi \qquad (8)$$

and

$$\phi = \frac{s}{R} , \qquad (9)$$

5
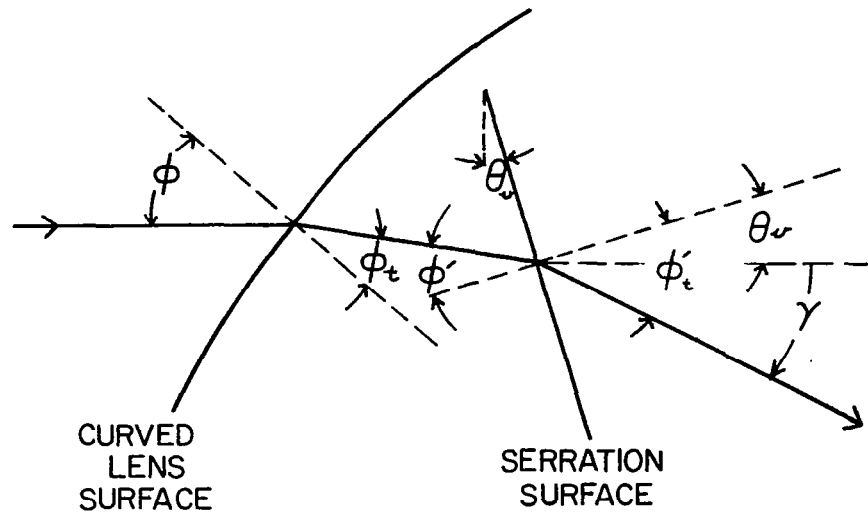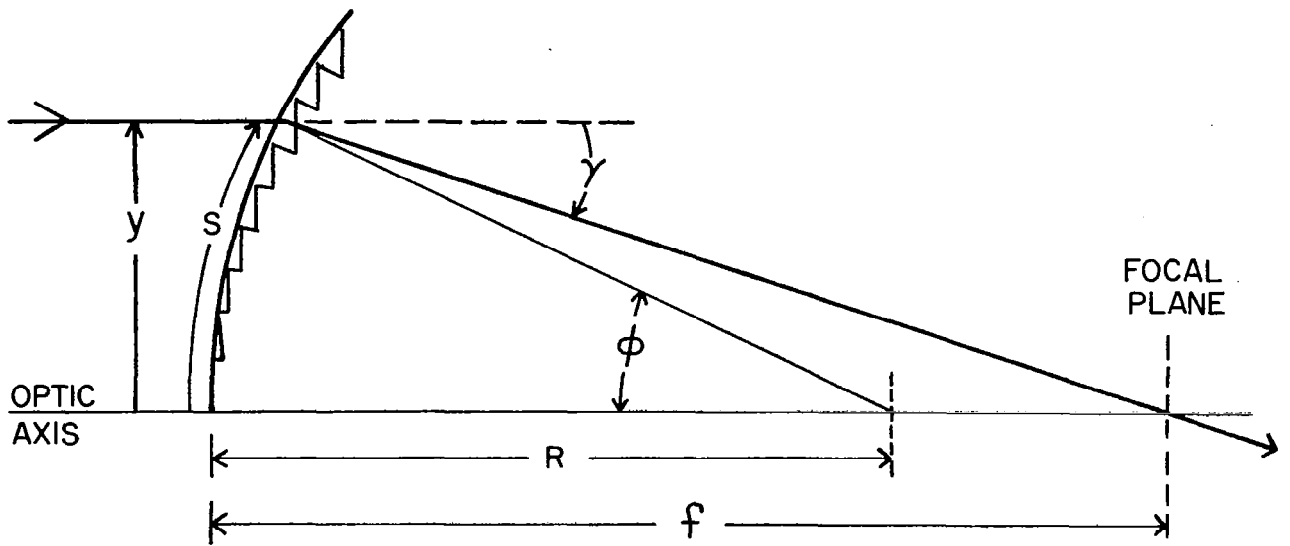
Figure 2. Ray diagrams for incident collimated light of the design wavelength.

where s is the serration center position measured along the arc of the lens. The groove angle θ measured with respect to the lens surface and given by

$$\theta \simeq \phi + \theta_v \qquad (10)$$

is then determined from Equations (5) thru (10).

C. Transmission Characteristics

1. Transmission Coefficient

Transmission losses occur primarily through reflection at the air-lens boundaries and absorption within the lens material. Surface reflection losses are analyzed using the Fresnel formulae. Attenuation of solar flux by absorption, primarily occuring in the infrared and ultraviolet portions of the solar spectrum, is empirically modelled as described in detail in Reference 4. Serration edge losses such as from adjacent groove blocking and errant edge refraction are assumed negligible.

The transmission coefficient for a given serration and solar wavelength is written as the product of the Fresnel transmittance factors T_1 and T_2 for the first and second lens surfaces, respectively, and a bulk transmittance factor T_a [4]:

$$T = T_1 T_a T_2 \quad . \qquad (11)$$

Incident angles for rays from the solar source center and its extremities differ only by approximately ±16 minutes of arc. Thus it is sufficient to determine the product $T_1 T_2$ for rays from the sun's center. For a single boundary, the transmission coefficient is

$$T = \frac{\sin 2\, \phi_{inc} \sin 2\, \phi_{ref}}{2 \sin^2 (\phi_{inc} + \phi_{ref})} [1 + \sec^2(\phi_{inc} - \phi_{ref})] \quad , \quad (12)$$

where ϕ_{inc} and ϕ_{ref} are the angles of incidence and refraction, respectively. For a ray striking the center of a serration in the "upper" lens half (Figure 3), T_1 is evaluated using Equation (12) and

$$\phi_{inc} = \phi_i = \phi - \delta \quad , \tag{13}$$

$$\phi_{ref} = \phi_t = \text{Arcsin} \left[\frac{\sin (\phi - \delta)}{n} \right] \quad . \tag{14}$$

Here δ is the transverse tracking error and n the appropriate index of refraction. The second surface transmission coefficient T_2 is likewise determined with

$$\phi_{inc} = \phi' = \phi - \phi_t + \theta_v \quad , \tag{15}$$

and

$$\phi_{ref} = \phi_t = \text{Arcsin} (n \sin \phi') \quad . \tag{16}$$

Replacing $(\phi - \delta)$ by $(\phi + \delta)$ in Equations (13) and (14), T_1 and T_2 for serrations in the "lower" lens half result from application of Equation (12).

Evaluation of T_a for a given spectral interval using measured transmittance curves [4], Equation (11) then yields the desired transmission coefficient.

2. Serration Sunlight Transmittance

The energy in the solar spectral interval $\Delta\lambda_j$ transmitted by a serration (the ith) per unit time per unit length is given by the product of the incident energy per unit time per unit length and the serration transmission coefficient T_{ij}, as determined in the previous section. The incident flux on the lens surface depends on the lens curvature at the serration position and on lens orientation, i.e., the tracking

8

CENTRAL
SOLAR
RAY

ϕ_i

ϕ

δ

θ_v

ϕ_t

ϕ'

ϕ'_t

CURVED
LENS
SURFACE
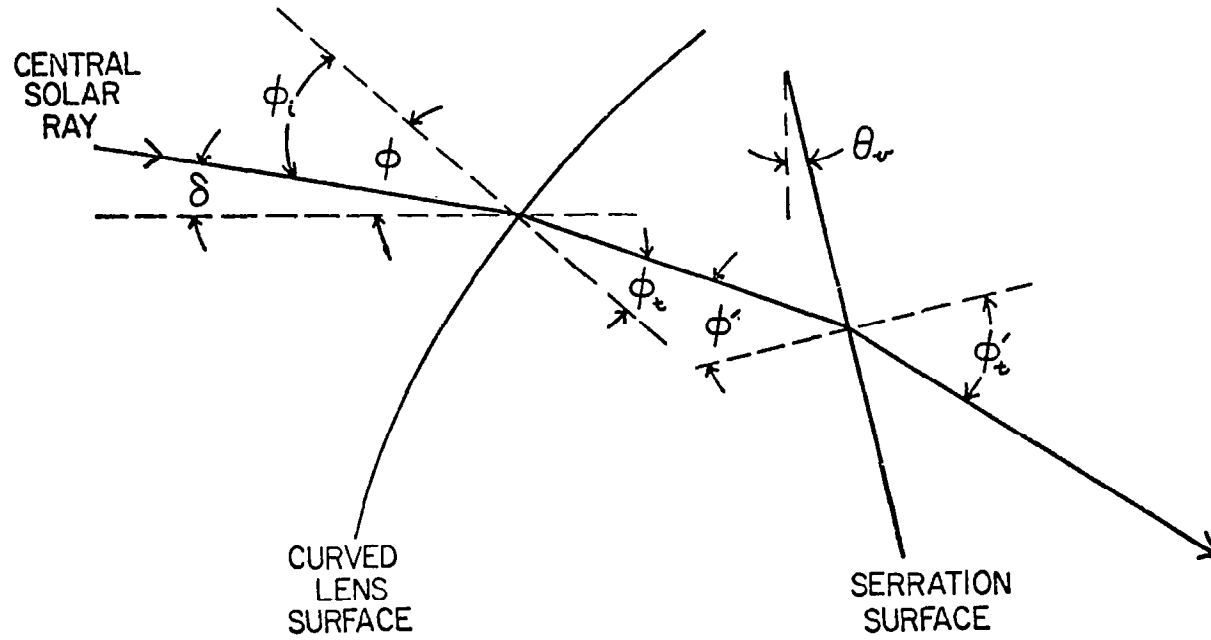
SERRATION
SURFACE

Figure 3. Ray diagram for light from the sun's center; transverse tracking
error δ present.

errors present. Simple geometrical considerations yield for the solar energy in the $(\Delta\lambda)_j$ spectral interval incident on the ith serration per unit time per unit length:

$$\text{Incident energy} = 2\ q_j\ R\ \sin\ \left[\frac{(\Delta s)_i}{2\ R}\right]\ \cos\ z_i\ , \qquad (17)$$

where q_j is the solar flux in the jth solar spectral interval, $(\Delta s)_i$ is the arc width of the ith serration, and

$$z_i = \phi - \delta \ , \ \text{upper lens half};$$
$$\qquad (18)$$
$$z_i = \phi + \delta \ , \ \text{lower lens half}.$$

Thus the solar energy in the $(\Delta\lambda)_j$ spectral interval transmitted by the ith serration per unit time per unit length is

$$\text{Transmitted energy} = \left\{2\ q_j\ R\ \sin\ \left[\frac{(\Delta s)_i}{2\ R}\right]\cos\ z_i\right\} \cdot T_{ij} \qquad (19)$$

Summing over the solar spectrum, the sunlight energy transmitted by the ith serration per unit time per unit length is

$$\begin{array}{l}\text{Transmitted}\\ \text{sunlight}\\ \text{energy}\end{array} = \sum_j \left\{2\ R\ \sin\left[\frac{(\Delta s)_i}{2\ R}\right]\cos\ z_i\right\} \cdot q_j\ T_{ij}\ . \qquad (20)$$

The serration sunlight transmittance T_i is the ratio of the transmitted to total incident solar flux. The total incident solar flux on the serration per unit time per unit length is

$$\text{Total incident flux} = 2\ q\ R\ \sin\ \left[\frac{(\Delta s)_i}{2\ R}\right]\cos\ z_i\ , \qquad (21)$$

with q the total solar insolation. T_i reduces to

$$T_i = \sum_j \omega_j\ T_{ij}\ , \qquad (22)$$

where the relation

$$q_j = \omega_j\ q \qquad (23)$$

has been used. Here ω_j is a spectral weighting factor [4].

3. Solar Spectral Transmittance

The transmitted fraction A_j of incident solar flux in the jth spectral interval is obtained by summing the contributions in Equation (19) over all lens serrations and dividing by the total energy in the jth interval incident on the lens per unit time per unit length $(q_j \; W \cos \delta)$:

$$A_j = \frac{\sum\limits_i \{2 \; R \; \sin[\frac{(\Delta s)_i}{2 \; R}] \cos z_i\} \; T_{ij}}{W \cos \delta} \quad .$$ (24)

4. Total Lens Transmittance

The total transmitted sunlight per unit time per unit length is evaluated by summing the contributions in Equation (19) over all lens serrations and all solar spectral intervals. Dividing by the incident energy on the lens $(q \; W \cos \delta)$, the total lens sunlight transmittance A is

$$A = \frac{2 \; R}{W \cos \delta} \sum_i \sum_j \{\sin[\frac{(\Delta s)_i}{2 \; R}] \cos z_i\} \; \omega_j \; T_{ij}$$ (25)

$$= \frac{2 \; R}{W \cos \delta} \sum_i T_i \; \sin[\frac{(\Delta s)_i}{2 \; R}] \cos z_i$$ (26)

$$= \sum_j \omega_j \; A_j \quad .$$ (27)

D. Concentrated Flux Distribution

The intensity of concentrated sunlight at a point beneath the lens can be determined by evaluating and adding intensity contributions from all lens serrations. For the geometry present, the intensity will not be a function of distance along the length axis of the lens. The problem therefore reduces to a one-dimensional determination of the intensity profile in the chosen

11

image plane normal to the length axis. Defining L_{ij} as the beam spread width in the image plane beneath the concentrator and recalling the assumption of uniform distribution of solar flux within this width, the intensity contribution at distance Y from the optical axis for sunlight in the spectral interval $\Delta\lambda_j$ refracted by the ith serration is

$$I_{ij}(Y) = \frac{T_{ij} \cdot \{2 \, q_j \, R \, \sin[\frac{(\Delta s)_i}{2 \, R}]\cos z_i\}}{L_{ij}} \quad . \tag{28}$$

When the contributions in Equation (28) are summed over all lens serrations, the resultant equation yields the local concentration ratio due to the jth wavelength segment of the solar spectrum:

$$\frac{I_j(Y)}{q} = \sum_i \frac{I_{ij}(Y)}{q}$$

$$= 2 \, R \, \omega_j \sum_i \frac{T_{ij} \, \sin[\frac{(\Delta s)_i}{2 \, R}]\cos z_i}{L_{ij}} \quad . \tag{29}$$

If the summation is over all solar spectral intervals instead, the concentration ratio due to refraction of sunlight by the ith serration is determined:

$$\frac{I_i(Y)}{q} = \sum_j \frac{I_{ij}(Y)}{q}$$

$$= 2 \, R \, \sin[\frac{(\Delta s)_i}{2 \, R}]\cos z_i \sum_j \frac{T_{ij} \, \omega_j}{L_{ij}} \quad . \tag{30}$$

Summing the contributions $I_{ij}(Y)/q$ over all serrations and the solar spectrum yields the total local concentration ratio:

$$\frac{I(Y)}{q} = \sum_i \sum_j \frac{I_{ij}(Y)}{q}$$

$$= \sum_i \sum_j \frac{2 \, R \, \omega_j \, T_{ij} \, \sin[\frac{(\Delta s)_i}{2 \, R}]\cos z_i}{L_{ij}} \quad . \tag{31}$$

12

Using Equations (31), (29), and (30), the total intensity profile, its spectral components, and individual serration profile contributions may be studied, provided the beam spread width L_{ij} for each wavelength and each serration is known. The intercepts in the image plane for rays from the extremities of the solar source refracted and exiting at the edges of individual serrations determine the L_{ij}.

Referring to the ray diagrams in Figures 4 and 5 for a serration on the sun side of the imperfectly tracking lens ("upper" lens half), the beam spread width is

$$L = Y1 - Y2 \quad , \tag{32}$$

where Y1 and Y2 are the extreme ray intercepts. Using the law of refraction and simple geometry,

$$Y1 = y_t - x_t \tan \gamma_t \quad , \tag{33}$$

where the ray exit coordinates (x_t, y_t) are

$$x_t \simeq f + d - (R - \sqrt{R^2 - y_t^2}) \tag{34}$$

$$y_t \simeq R \sin \beta_t , \tag{35}$$

with d a defocus parameter and

$$\beta_t = \frac{s + (\Delta s)/2}{R} \quad ; \tag{36}$$

$$\gamma_t = \text{Arcsin} [n \sin (\beta_t - \phi_t + \theta_v)] - \theta_v \quad ; \tag{37}$$

$$\phi_t = \text{Arcsin} \left[\frac{\sin (\beta_t - \delta + \alpha)}{n}\right] \quad . \tag{38}$$

The angle 2α is the apparent angular diameter of the Sun.
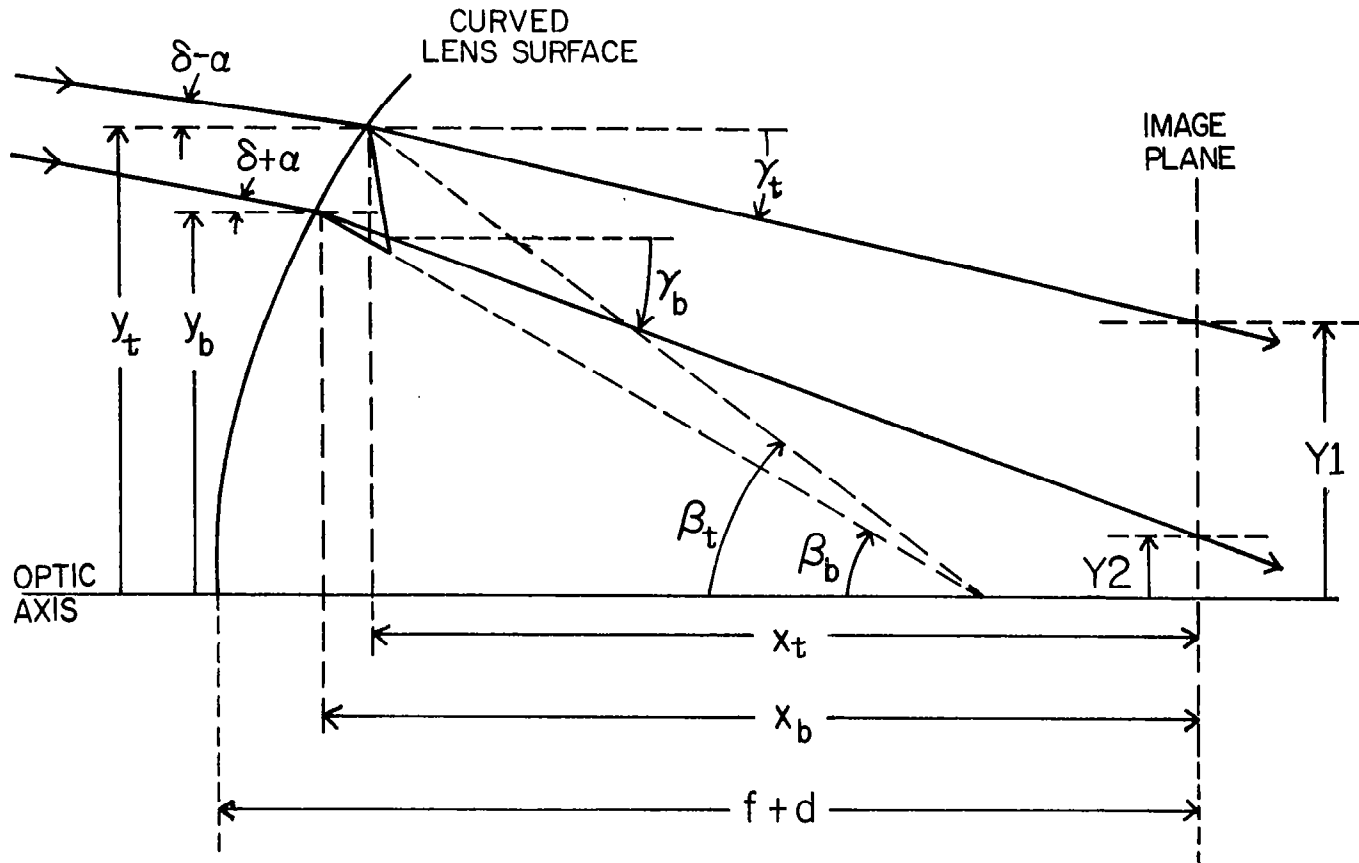
Figure 4. Ray tracing of sunlight from solar extremities thru serrations on sun side of an imperfectly tracking curved lens.
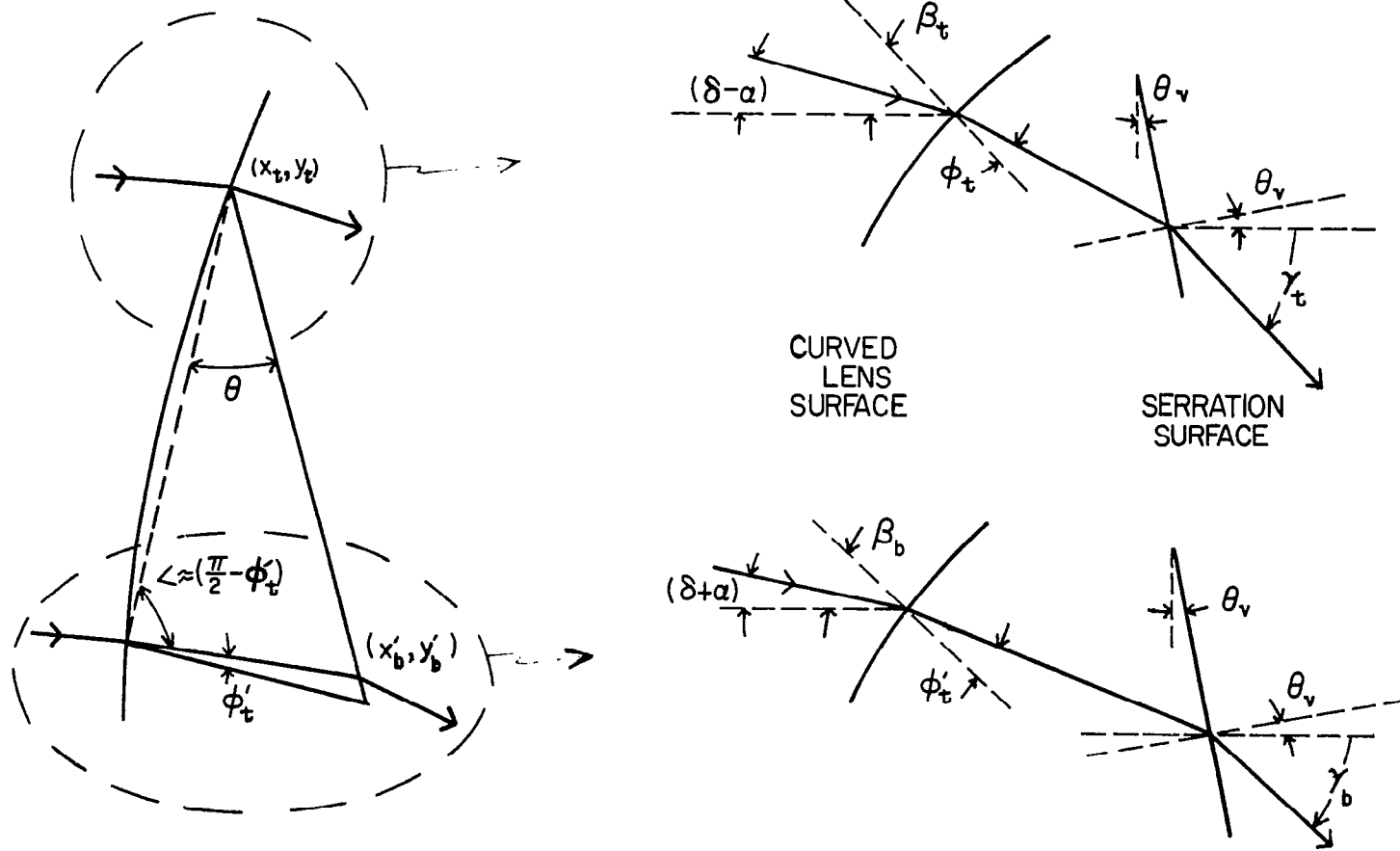
Figure 5. Extreme ray refraction details.

Similarly,

$$Y2 = y_b' - x_b' \tan \gamma_b \quad , \tag{39}$$

where, using Figure 5, the ray exit coordinates are approximately

$$x_b' \simeq x_b - \frac{(\Delta s) \sin \theta \cos (\beta_b - \phi_t')}{\cos (\phi_t' - \theta)} \quad , \tag{40}$$

$$x_b \simeq f + d - (R - \sqrt{R^2 - y_b^2}) \quad , \tag{41}$$

$$y_b \simeq R \sin \beta_b \quad , \tag{42}$$

$$\beta_b = \frac{s - (\Delta s)/2}{R} \quad ; \tag{43}$$

$$\phi_t' = \text{Arcsin} \left[\frac{\sin (\beta_b - \delta - \alpha)}{n} \right] \quad ; \tag{44}$$

and

$$y_b' \simeq y_b - \frac{(\Delta s) \sin \theta \sin (\beta_b - \phi_t')}{\cos (\phi_t' - \theta)} \quad ; \tag{45}$$

$$\gamma_b = \text{Arcsin} \left[n \sin (\beta_b - \phi_t' + \theta_v) \right] - \theta_v \quad . \tag{46}$$

For serrations in the lower lens half,

$$L = Y3 - Y4 \quad , \tag{47}$$

with Y3 and Y4 designating the extreme ray intercepts. Using Figures 6 and 7

$$Y4 = - (y_t - x_t \tan \gamma_t') \quad , \tag{48}$$

where from Figure 7 and Snell's law of refraction,

$$\gamma_t' = \text{Arcsin} \left[n \sin (\beta_t - \phi_b + \theta_v) \right] - \theta_v \quad , \tag{49}$$

with

$$\phi_b = \text{Arcsin} \left[\frac{\sin (\beta_t + \delta + \alpha)}{n} \right] \quad . \tag{50}$$

16
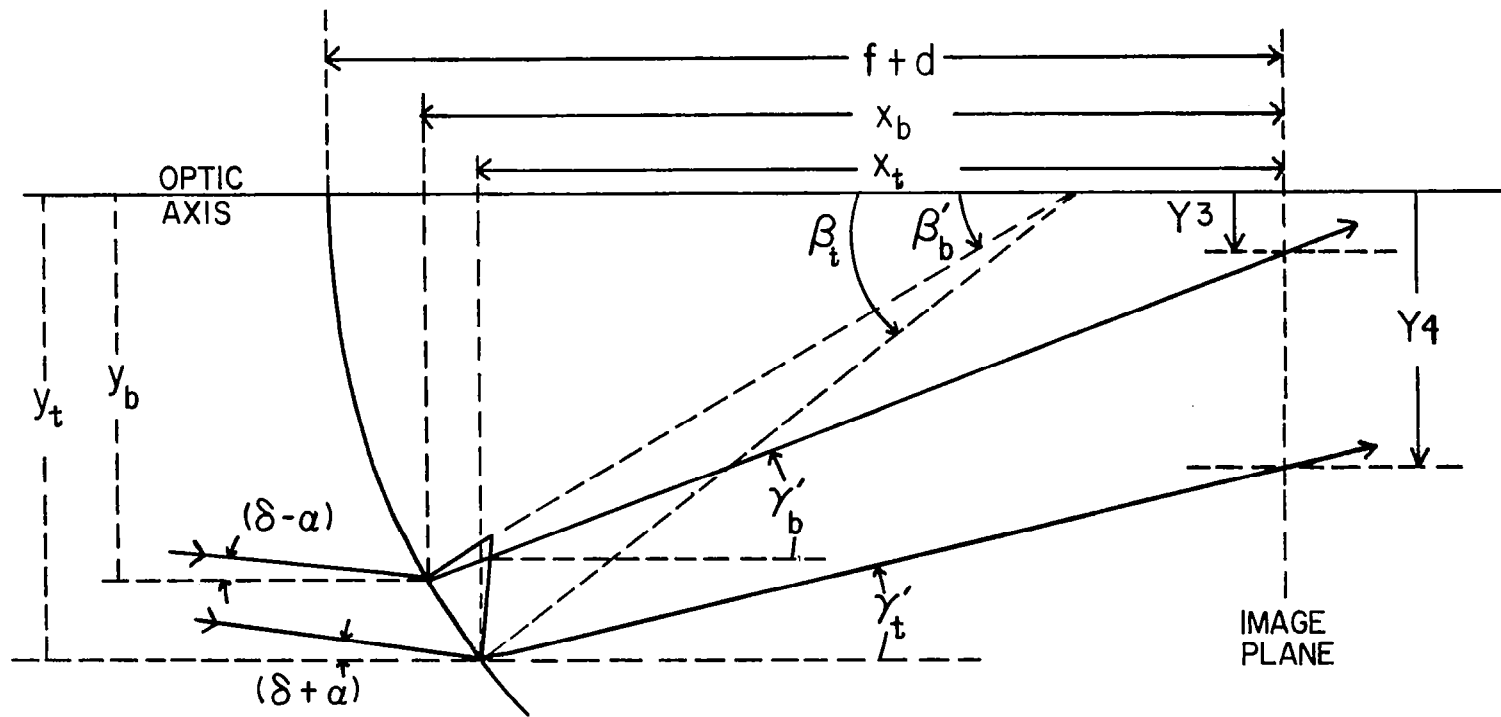
Figure 6. Ray tracing of sunlight from solar extremities thru serrations on lower side of an imperfectly tracking curved lens.
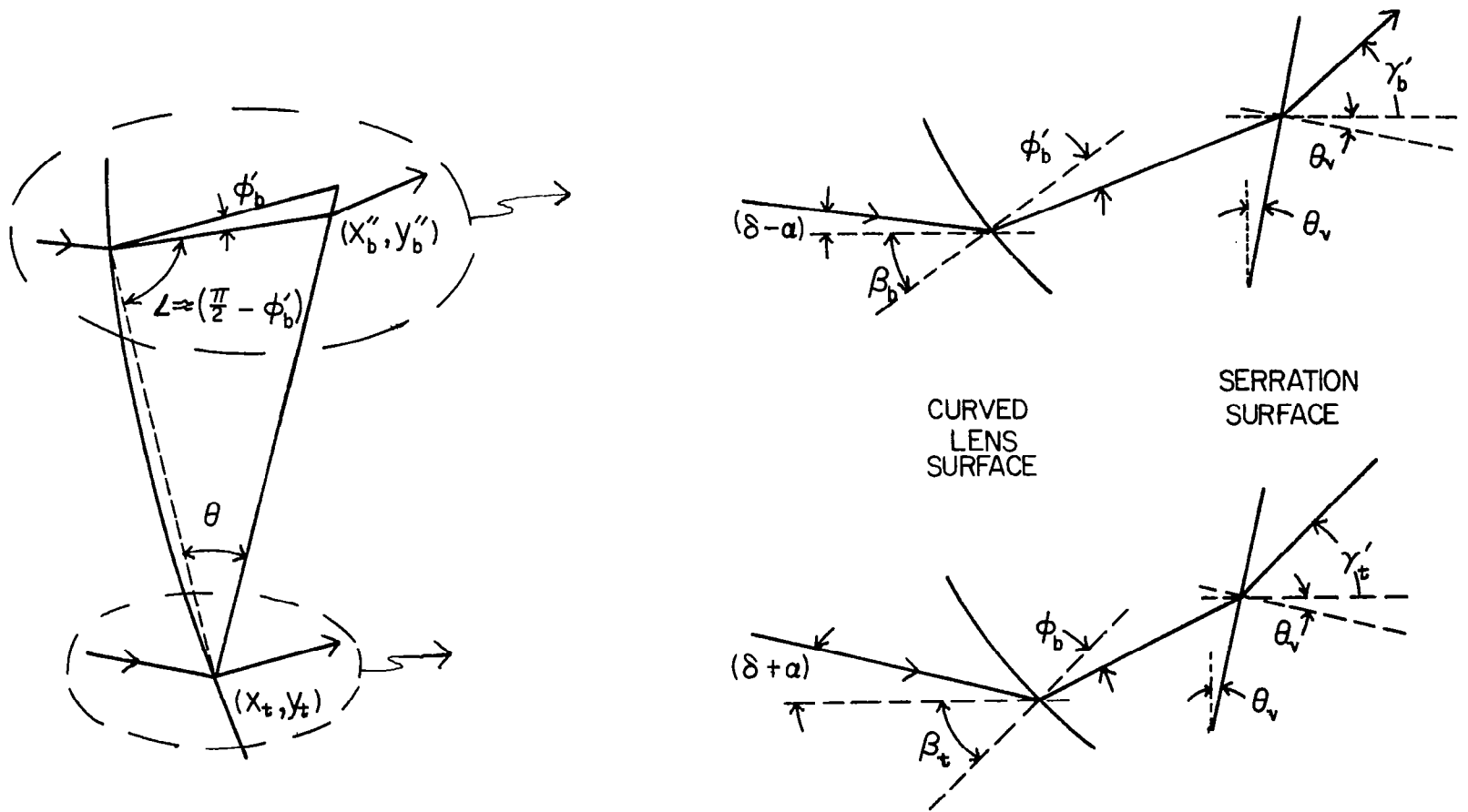
Figure 7. Extreme ray refraction details.

Also, for the other intercept

$$Y3 = -(y_b'' - x_b'' \tan \gamma_b') \quad . \tag{51}$$

From Figure 7, the ray exit coordinates (x_b'', y_b'') are approximately

$$x_b'' \simeq x_b - \frac{(\Delta s) \sin \theta \cos (\phi_b' - \beta_b)}{\cos (\phi_b' - \theta)} \quad ; \tag{52}$$

and

$$y_b'' \simeq y_b + \frac{(\Delta s) \sin \theta \sin (\phi_b' - \beta_b)}{\cos (\phi_b' - \theta)} \tag{53}$$

Now

$$\phi_b' = \text{Arcsin} \left[\frac{\sin (\beta_b + \delta - \alpha)}{n}\right] \quad . \tag{54}$$

Also,

$$\gamma_b' = \text{Arcsin} [n \sin (\beta_b - \phi_b' + \theta_v)] - \theta_v \quad . \tag{55}$$

For the above ray tracing, the thickness of the lens base is assumed negligible. The serration height is considered, however, by determining ray exit positions near the serration tip. In evaluating the ray exit positions (x_b', y_b') and (x_b'', y_b''), the serration arc lengths Δs and the associated chord lengths (Figures 5 and 7) are assumed equal. Further, the angle between the normal to the curved surface and the chord is approximated as $\pi/2$. Thus the ray exit positions are approximations.

For a given set of lens parameters, transverse tracking error, and image plane, Equations (32) thru (55) can be used to compute beam spread widths and hence permit study of the intensity profile and its components.

19

III. THEORETICAL RESULTS AND DISCUSSION

A. Introduction

Based on the preceding lens model, a Fortran-10 computer program has been used to develop example performance data for a curved, line-focusing Fresnel lens. The effects of curvature, f-number (ratio of focal length to aperture width), transverse tracking errors, and defocusing on the solar transmittance and imaging characteristics of a lens concentrator have been evaluated.

Since low f-numbers are particularly of interest, computations have been performed for lenses with f-numbers in the range f/0.7 to f/1.0. (The focal lengths are measured from the lens vertex.) Selected curvature radii range from infinite (flat lens) to as low as one half the focal length. Curvature radii are expressed in terms of the focal lengths to facilitate possible identification of an optimum lens curvature, as indicated in a preliminary study.

Performance sensitivities to small transverse tracking errors are studied over the range 0°-2° and for a variety of f-numbers and curvatures. Image profile changes with slight defocusing are investigated for the range -2% to + 2% of the focal length, again for various focal lengths and curvature radii. Negative percentages represent image plane shifts toward the lens from the design focal plane and positive percentages are for image planes shifted away from the lens and design focal plane.

For solar concentrators, the primary objective is the interception, transmission, and image plane localization of solar energy, as previously indicated. Performance comparisons can be based on the width of a target receptor centrally located in an image plane that is required to intercept a given fraction of the sunlight energy incident on the concentrator.

Conversely, the fraction of incident energy received by a target of given width can be studied and compared for various concentrator parameters, depending on whether the target receptor is designed for the concentrator or vice versa.

In the present study, lens performances are primarily assessed and compared using "normalized" target receptor widths, i.e., most target widths are expressed as a ratio with respect to the equivalent focal plane target width for an f/1.0 flat lens with perfect tracking. Performance details include lens transmission characteristics and image features such as peak concentration ratios, peak position shift, and profile asymmetry.

Following a discussion of lens and spectral parameters employed and the computations of required groove angles, computer-generated analytical data on curved lens performance are presented and discussed in this section.

B. Lens and Spectral Parameters

Example lens characteristics are specified in Table 1. The 36 inch width, acrylic material, and 25 per inch groove density are believed reasonable choices for an actual concentrator. For other lens widths, the concentration performance should be equivalent, with roughly only scale changes involved.

It should also be noted that the choice of a constant arc groove density (perhaps the simplest choice for both analytical studies and actual lens fabrication) results in an increasing number of lens serrations as the curvature increases. The "cross-sectional" groove density increases outwardly from the lens center. Thus any changes in lens performance due to this groove geometry are included in the "curvature" effects.

As in previous studies on flat base Fresnel lens concentrators [3-5], Moon's solar radiation data [6] was utilized to determine the weighting factors for the intervals in the selected solar spectral dissection (twenty-

TABLE 1. EXAMPLE LENS CHARACTERISTICS

Lens Type	Curved Base, Line Focusing Fresnel, Grooves Down
Material	Acrylic
Width	36 inches (91.4 cm)
Arc Groove Density	25.4 in^{-1} (10 cm^{-1})
Design Index of Refraction	1.49

TABLE 2. SOLAR AND LENS SPECTRAL PARAMETERS

Wavelength Increment $(\Delta\lambda)_j$ (microns)	Center Wavelength λ_j (microns)	Weighting Factors ω_j	Acrylic Index of Refraction n_j	Acrylic Bulk Transmittance Factor $(T_a)_j$
0.295-0.40	0.374	2.67×10^{-2}	1.5250 (estimate)	0.675
0.40-0.43	0.416	2.75	1.5155	0.995
0.43-0.45	0.441	2.44	1.5018	1
0.45-0.47	0.460	2.91	1.4999	1
0.47-0.49	0.480	3.20	1.4982	1
0.49-0.51	0.500	3.27	1.4968	1
0.51-0.53	0.520	3.23	1.4954	1
0.53-0.55	0.540	3.22	1.4942	1
0.55-0.57	0.560	3.19	1.4930	1
0.57-0.60	0.585	4.73	1.4918	1
0.50-0.63	0.615	4.73	1.4906	1
0.63-0.66	0.645	4.75	1.4895	1
0.66-0.69	0.675	4.56	1.4886	1
0.69-0.73	0.709	5.37	1.4876	1
0.73-0.78	0.753	5.91	1.4865	1
0.78-0.83	0.804	5.62	1.4854	1
0.83-0.89	0.857	6.23	1.4845	1
0.89-0.99	0.953	6.06	1.4832	1
0.99-1.06	1.024	5.65	1.4826	1
1.06-1.21	1.129	6.21	1.4818	0.948
1.21-1.52	1.274	6.49	1.4812 (estimate)	0.912
1.52-2.2	1.642	6.81	1.4808 (estimate)	0.570

two divisions). Appropriate indices of refraction and bulk transmittance factors for the solar spectral intervals (Table 2) were obtained from manufacturer's acrylic dispersion data and transmission curves [7].

C. Groove Angles

Required groove angles have been computed for various example lenses using Equations (5) thru (10). Measured with respect to the lens surface, the groove angles increase as the serration arc position moves outward from the lens center, as illustrated in Figure 8 for an f/1.0 flat example lens. By comparing this curve with Figure 9 for a curved lens (R/f = 0.7) with an identical focal length, the general increase in the maximum groove angle with increasing curvature is demonstrated. For lower f-numbers, the maximum groove angle increases further, reaching, e.g., approximately 65° for an f/0.8, R/f = 0.7 lens (Figure 10).

These large angles are necessitated by the two-surface refraction of incident parallel rays by the curved lens. Such large angles in a flat base lens results in total internal reflection of incident light.

D. Lens Transmission Characteristics

1. Serration Sunlight Transmittances

The transmittance of sunlight by individual lens serrations, as computed using Equation (22), is a slow varying function of serration arc position. As illustrated in Figure 11 for a perfectly tracking f/0.8, R/f = 0.8 lens, sunlight transmittance varies from about 88% near the lens center to 83% for the outer lens grooves.

The presence of small transverse tracking errors has little effect on serration sunlight transmittances, improving the transmittances for the lower lens half and decreasing the fractions slightly for upper

23
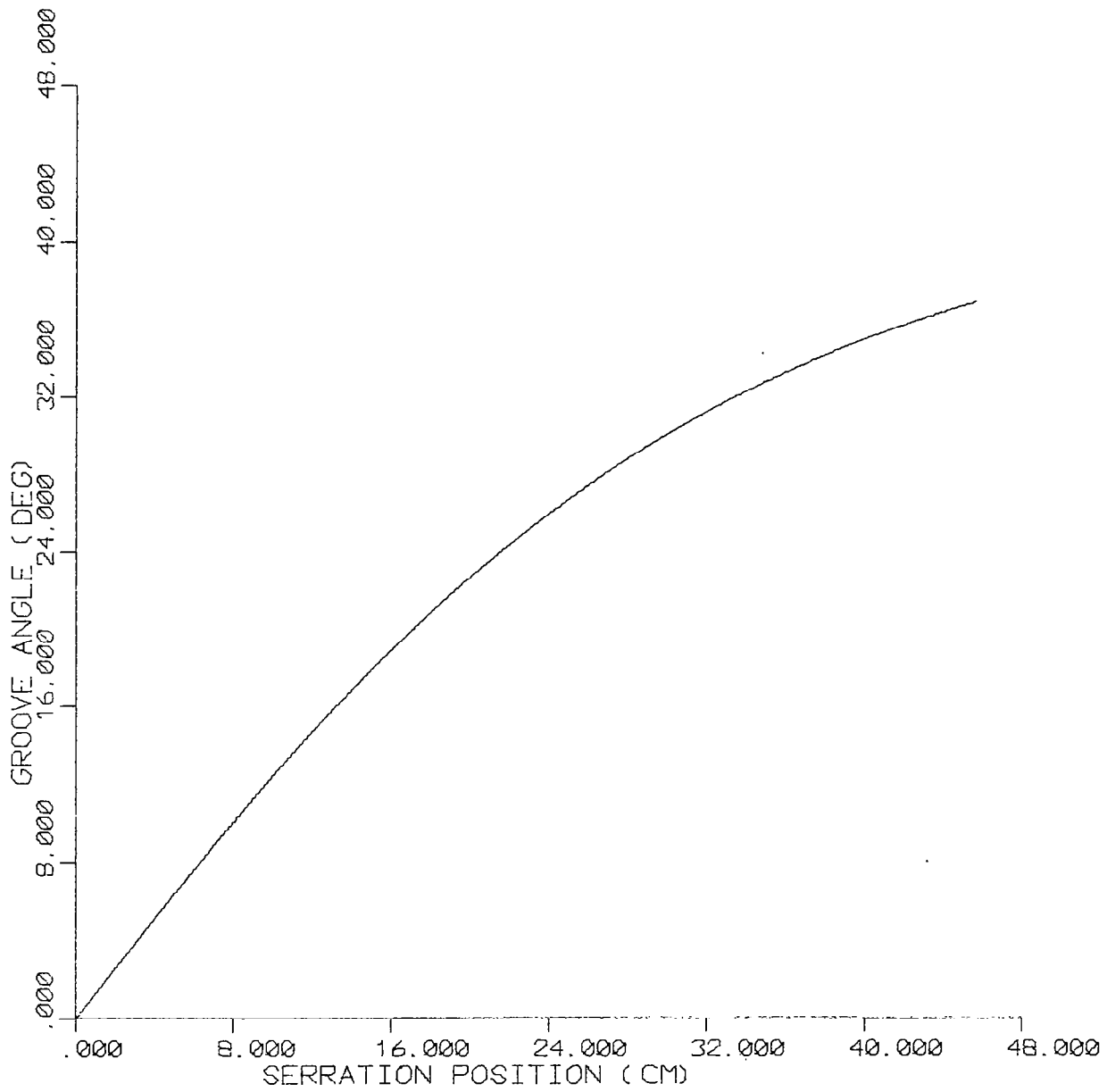
Figure 8. Groove angles for a flat, f/1.0 Fresnel lens.

24
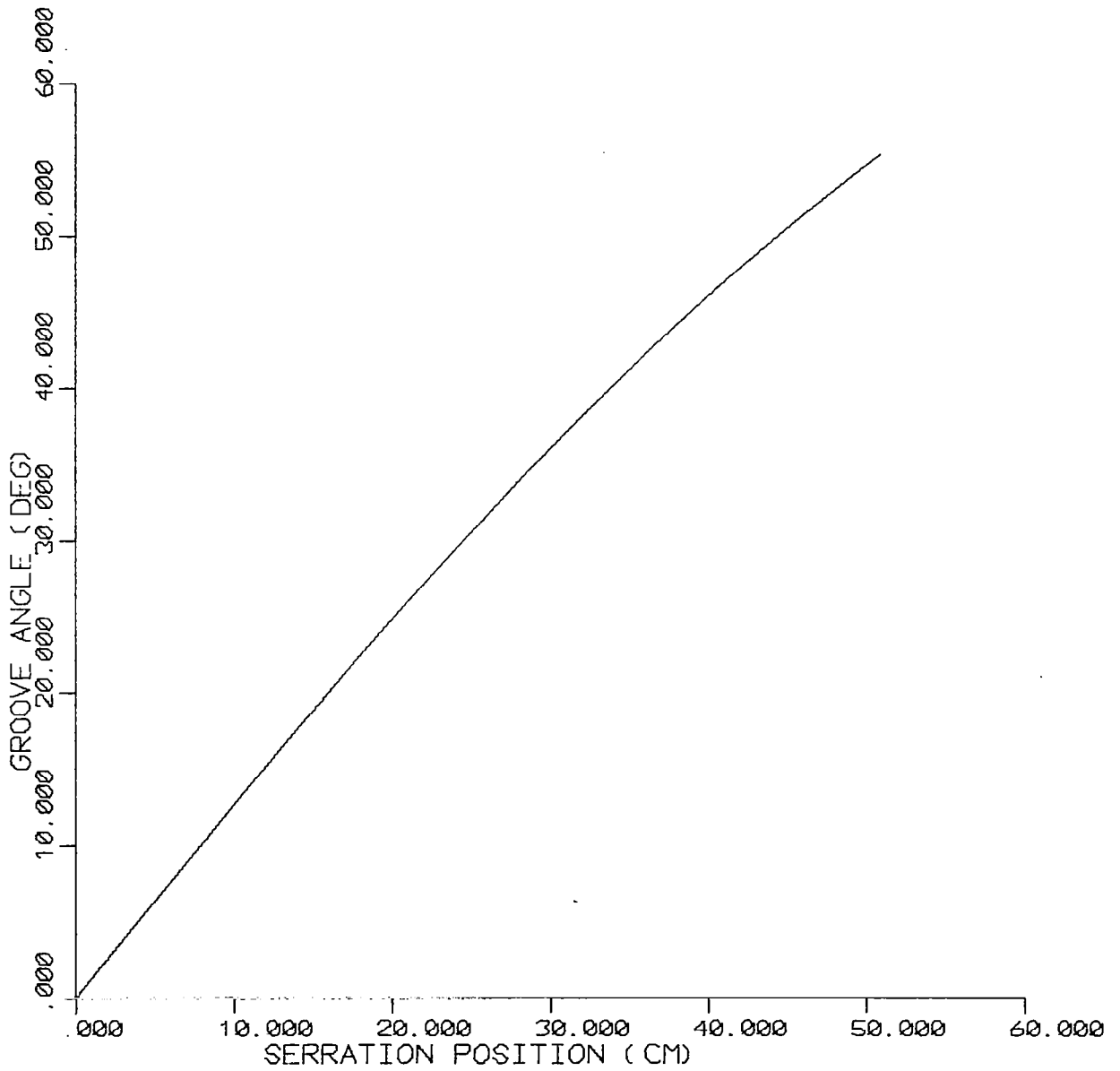
Figure 9. Groove angles for an f/1.0 curved lens; R/f = 0.7.
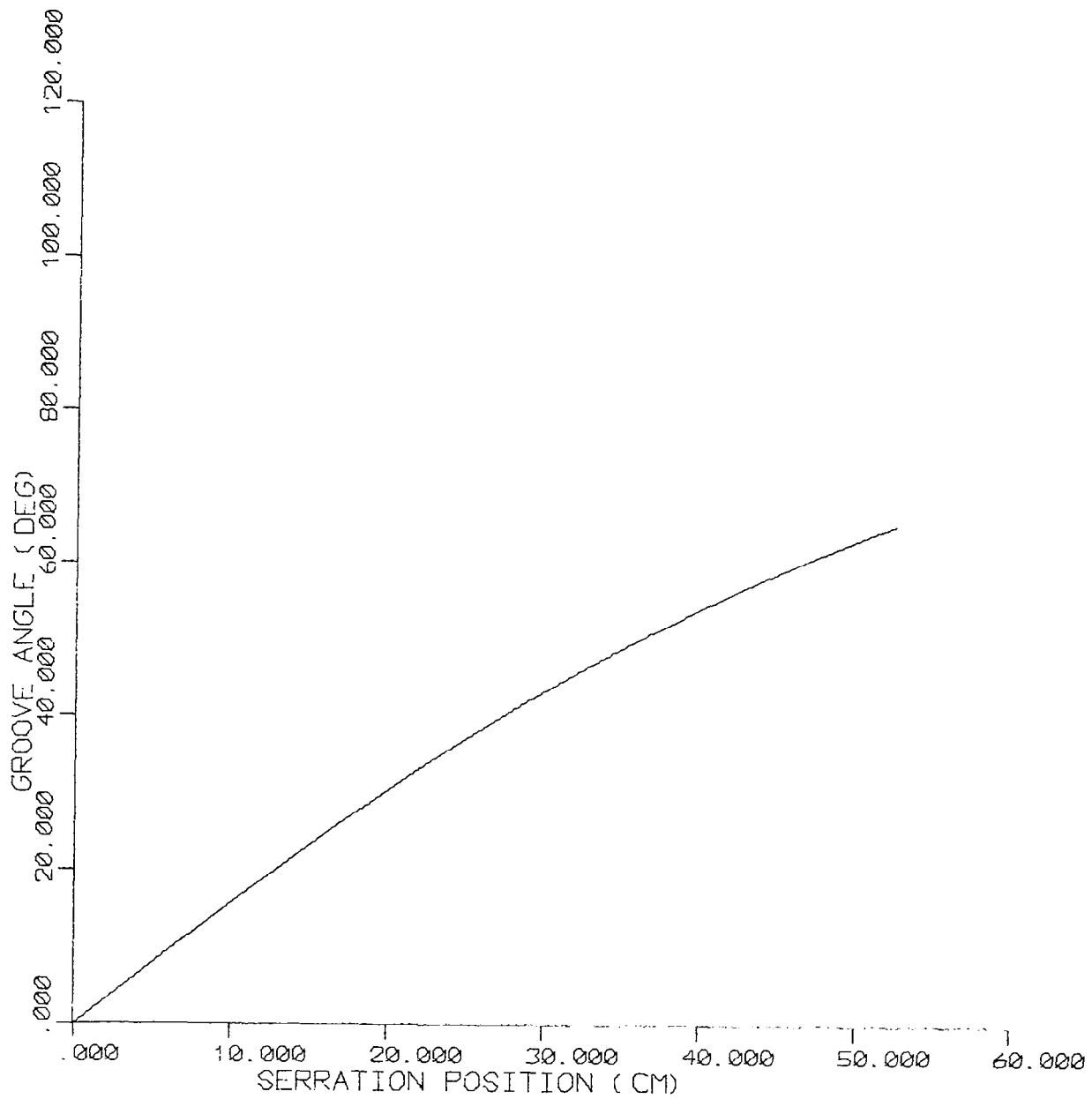
Figure 10. Groove angles for an f/0.8 curved lens; R/f = 0.7 .
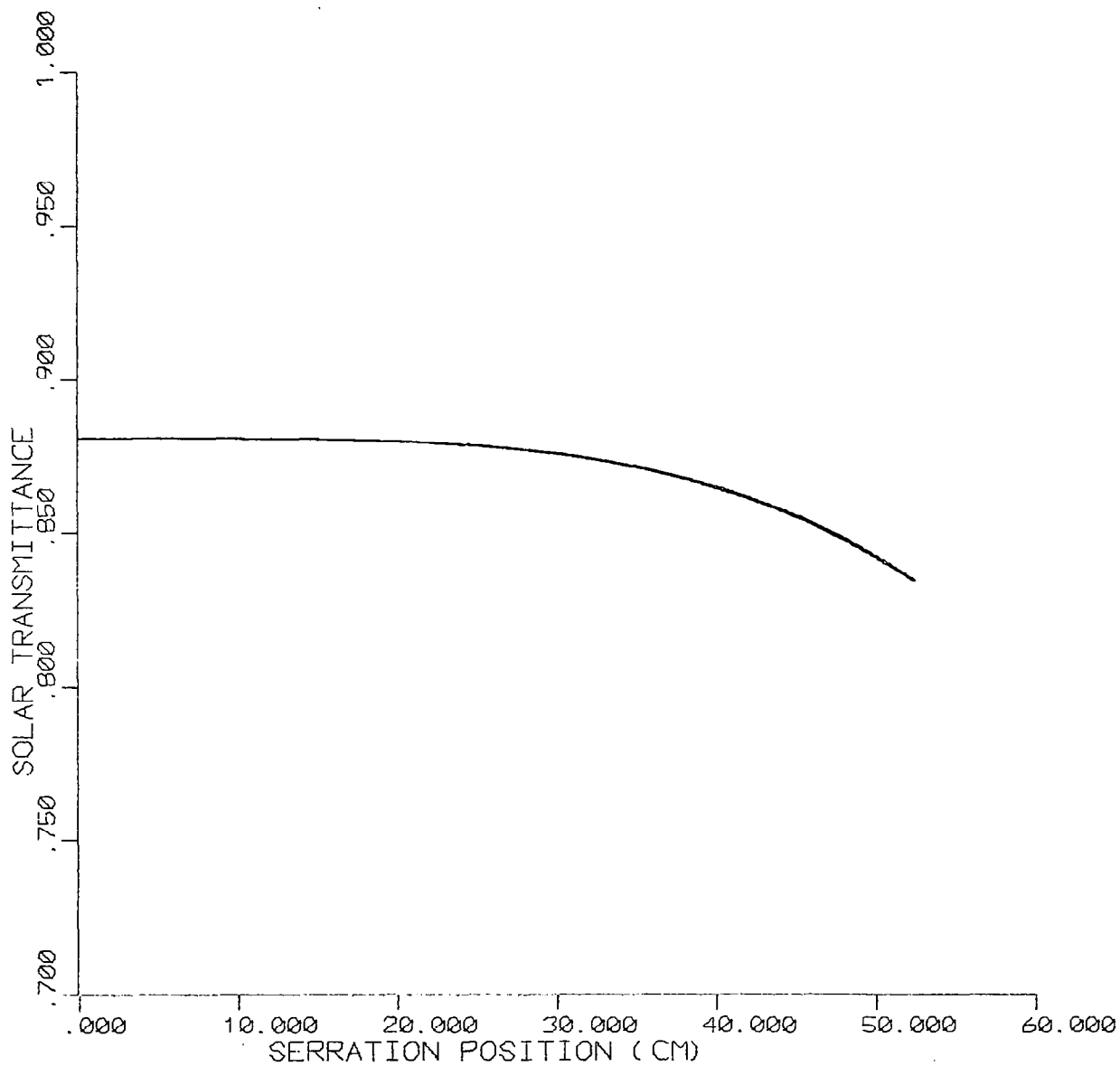
Figure 11.   Serration sunlight transmittance for an f/0.8 curved lens; R/f = 0.8.

27

half serrations. Figure 12 demonstrates this effect for the above lens
with a 2° transverse error.

2. Spectral Transmittances

Equation (24) provides for computations of spectral transmittances.
A typical variation of lens transmittance over the solar spectrum is
depicted in Figure 13 for a perfectly tracking f/0.8, R/f = 0.8 lens.
Low and high spectral indices refer to the UV and IR ends of the solar
spectrum, respectively. As expected, acrylic absorption in the ultra-
violet and infrared regions is substantial. In spectral regions where
absorption is negligible, the transmittance increases very slowly with
wavelength from roughly 91 to 92%. It should be noted that actual lens
absorption will vary somewhat with lens thickness. The bulk transmittance
factors used in the present computations correspond to roughly a quarter
inch thickness of acrylic [7].

3. Total Lens Transmittance

For the range of f-numbers, curvatures, and tracking errors considered,
the total lens transmittance, as computed using Equation (25), varied
from a low of 83.2% for a flat f/0.7 lens to a high of 87.8% for a
perfectly tracking f/1.0, R/f = 0.8 concentrator. Generally, transmit-
tance decreases slightly with decreasing f-number for lenses with
similar curvatures, e.g., the transmittance for an f/0.7, R/f = 1.0 lens
is 1.5% less than for an f/1.0 lens with the same radius of curvature.

The total lens transmittance as a function of lens curvature exhibits
a maximum for curvatures of roughly R/f = 0.8, with the more pronounced
maxima for low f-numbers. For example, the highest difference between
the maximum transmittance value and the flat lens transmittance, 3.1%,
occurs for an f/0.7 lens compared to a 1.1% difference for an f/1.0 lens.
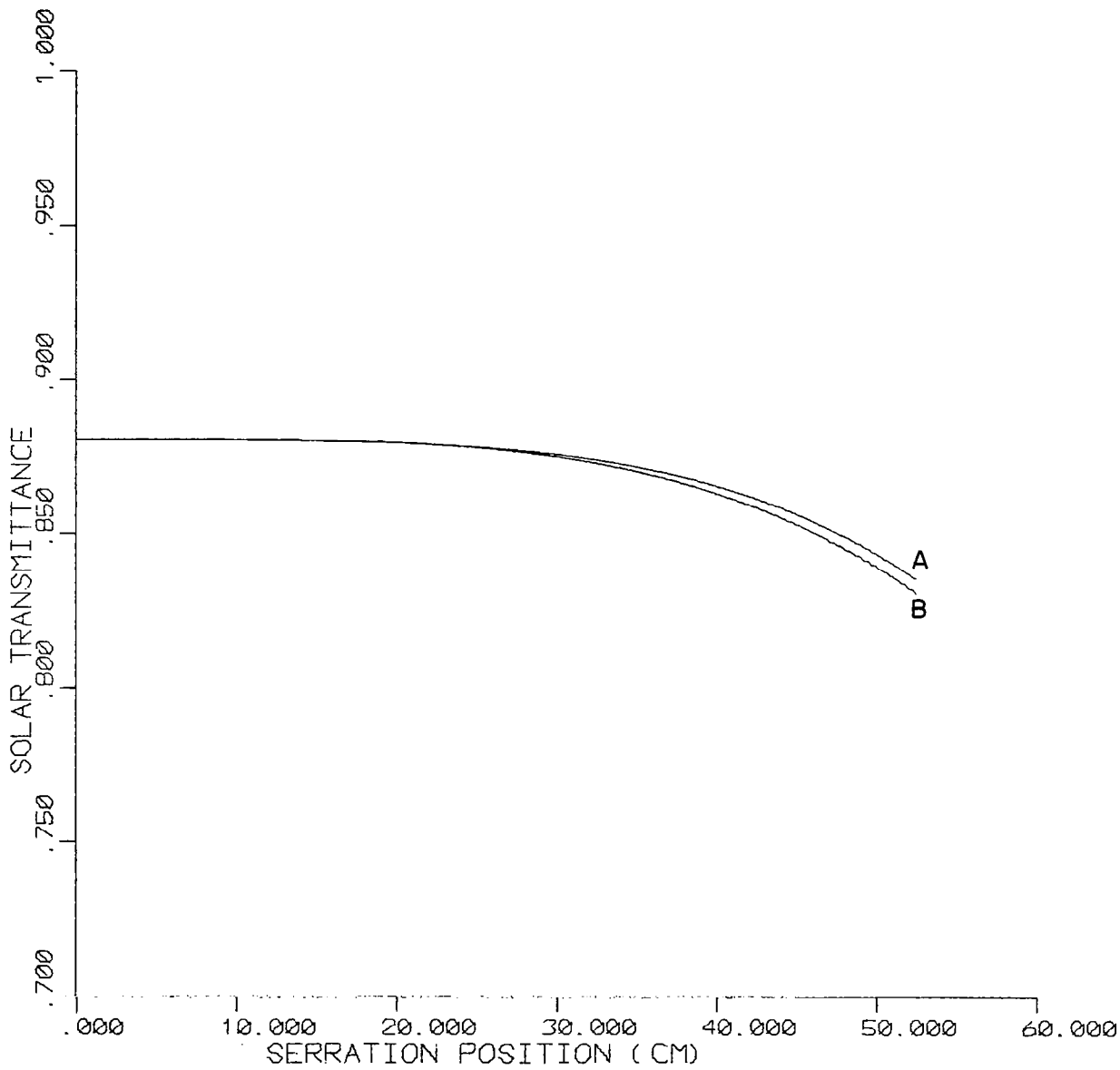
Figure 12. Serration sunlight transmittance for an f/0.8 curved lens with 2° tracking error; R/f = 0.8. A – lower half; B – upper half.

29
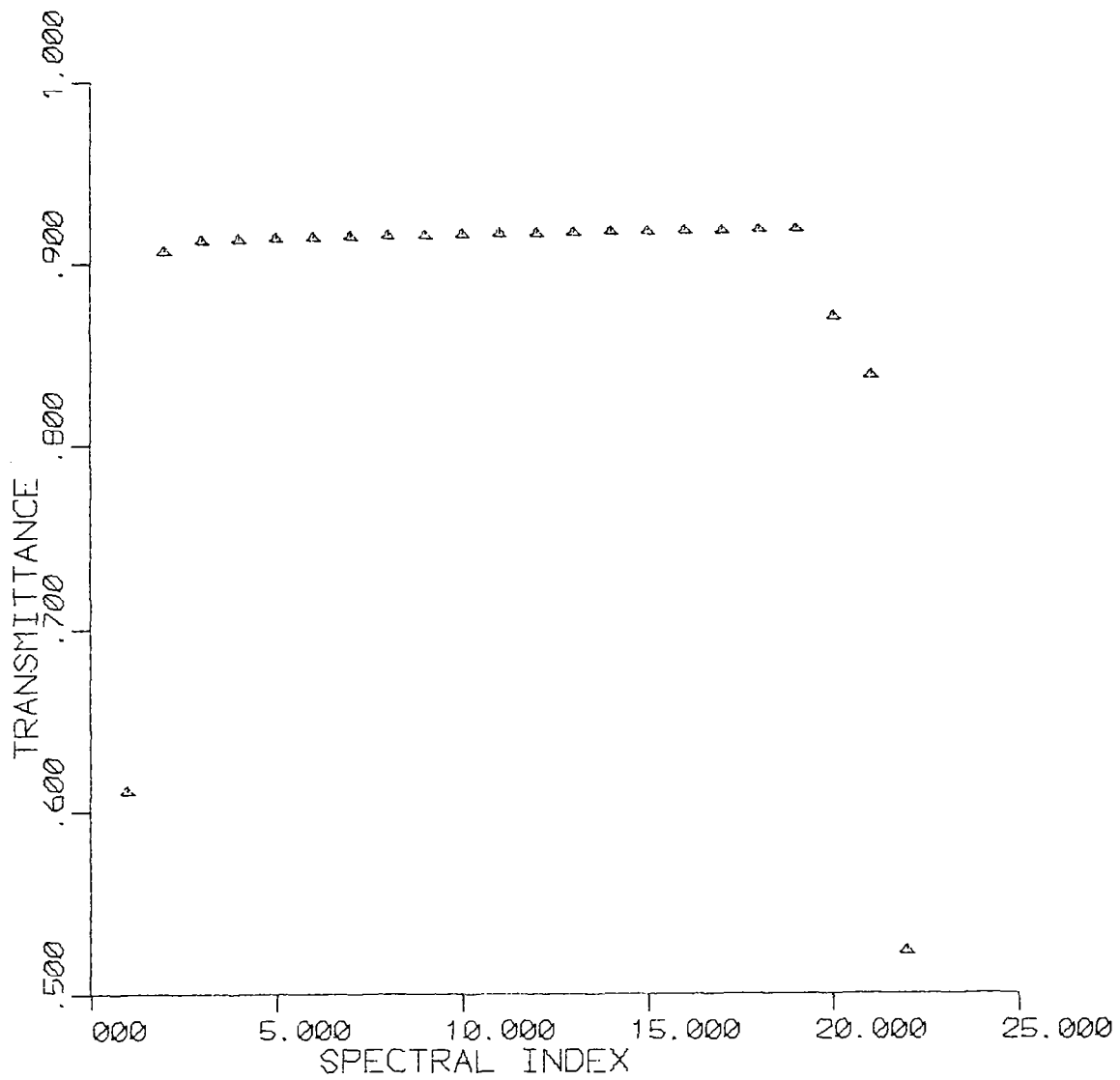
Figure 13. Lens spectral transmittances over the UV
to IR wavelength range of sunlight.

30

For transverse tracking errors $\leq 2°$, the total lens transmittance remained essentially unchanged (less than 0.1% variation) from the perfect tracking value for all cases investigated.

E.   Image Intensity Profiles

Profiles of concentrated flux are determined from application of Equation (31) to the example lens case. Computerized numerical integration is used to calculate, as a function of target width, the fraction of incident and/or transmitted flux intercepted by a target centrally located in the chosen image plane (e.g., see Figure 14 for a representative curve). The focal plane target width required to intercept 90% of the transmitted flux for a perfectly tracking f/1.0 flat lens is computed as 2.09 cm. (The focal plane image profile for this case is included in Fugure 17). Because the lens transmittance is 86.7%, this corresponds to a 78% interception of the sunlight energy incident on the lens. To facilitate comparison of concentrator performances in the following studies of curved lens solar imaging characteristics, the primary evaluation tool is selected as the width of a centrally located target required to intercept 78% of the solar flux incident on the lens. This target width is expressed as a ratio with respect to the f/1.0 flat lens value of 2.09 cm.

Note that other intercept percentages could be chosen as the basis for target width computations. However, the performance sensitivity comparisons and basic conclusions should be the same. The 78% intercept figure is believed to be a reasonable design requirement for target receptors beneath lenses which achieve or approximate the theoretical transmittances discussed earlier.

31
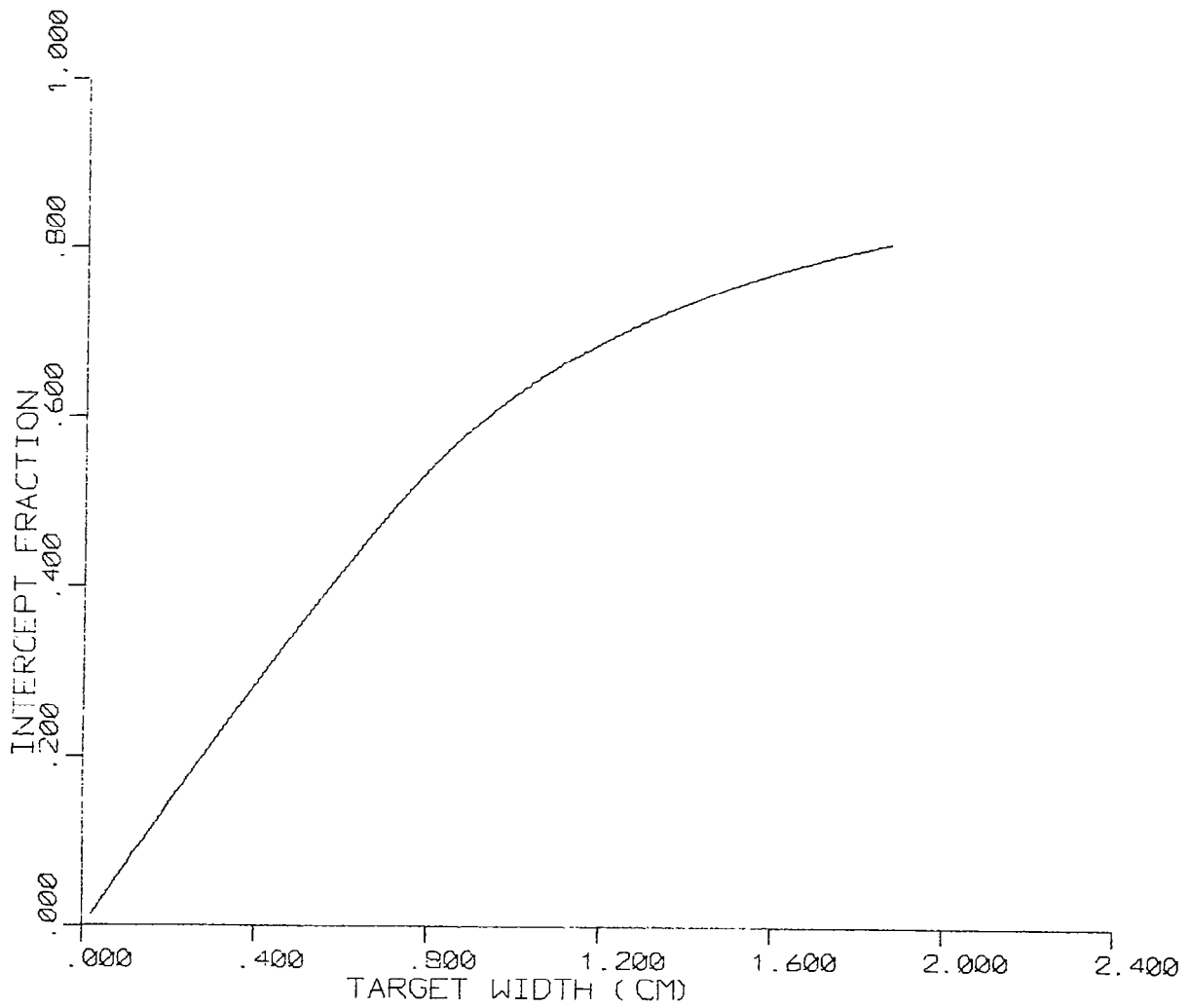
Figure 14. Fraction of incident sunlight intercepted by a symmetrically located target in the focal plane of an f/1.0 lens with R/f = 0.7.

32

1. Focal Plane Concentration - F-Number and Curvature Sensitivities

Focal plane image profiles for perfectly tracking lenses were computed for f-numbers of 1.0, 0.9, 0.8, and 0.7. For each f-number, intensity curves were examined for various curvature radii ranging from the flat lens (infinite curvature radius) to near the minimum radius of curvature (one half the lens width). The results are summarized in Figure 15 where the target width ratio is plotted versus the radius of curvature, expressed as a ratio with respect to the concentrator focal length. Several observations on the performance sensitivities to f-number and curvature can be made.

First, it is evident from Figure 15 that curving the base of a Fresnel lens solar concentrator significantly reduces the required focal plane target width. For example, a 25% decrease in target width over the flat lens value is possible for an f/1.0 lens if the curvature ratio R/f = 0.6 is achieved. This increased localization of concentrated sunlight raises the peak concentration value from 59 to 68. Similar changes in target width and peak concentration occur with increasing curvature for lower f-number lenses, with peak concentration vlaues as high as 73.

Secondly, only the f/0.7 data exhibits a minimum, indicating an optimum curvature for solar concentration near the value R/f = 0.8. Tendencies toward minima are observed for the f/0.8 and f/0.9 data, also due to a decreasing lens transmittance. Relatively small decreases in lens transmittances for small R/f values would cause the appearance of minima. However, within the assumptions and limitations of the present analytical model, the optimum curvature radius is evidently at or near the minimum radius.
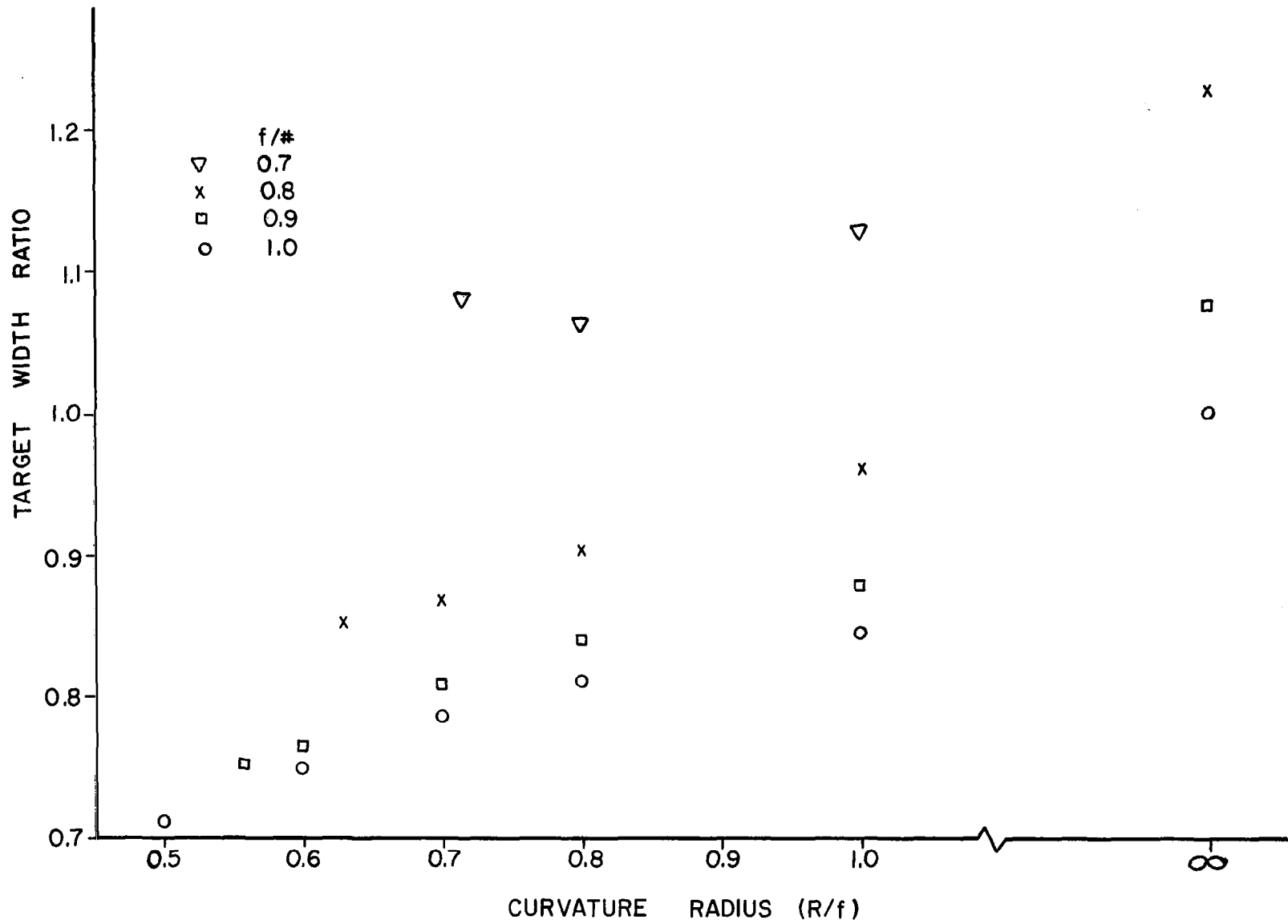
Figure 15. Solar performance sensitivities to lens curvature and f-number. Target widths computed for focal plane of perfectly tracking lens.

Third, the lower the f-number, the larger the required target width if lenses of similar curvatures are compared. It is interesting to note that lenses with f-numbers f/0.8 or larger and curvature radii R/f ≤ 1 all exhibit lower target widths than the f/1.0 flat lens. Therefore, by using curved base lenses, both an increase in concentrator optical performance and a decrease in structural size of the concentrator - receptor system is possible, relative to the f/1.0 flat lens case.

2. Transverse Tracking Error Sensitivities

Focal plane image profiles were investigated for transverse tracking errors of 0°, 0.25°, 0.5°, 1° and 2° for a variety of f-numbers and lens curvatures. As illustrated in Figure 16 for an f/1.0 lens, curving the lens base decreases the target width and its rate of increase with transverse error. This improvement results partially from a dramatic decrease in profile skewness for the larger tracking errors, as seen by comparing the image profiles in Figures 17 and 18 for a flat, f/1.0 lens and in Figure 19 for an R/f = 0.7 lens with the same focal length. For the curved lens, profile asymmetry increases as the curvature radius is decreased. For example, compare the intensity profile for a tracking error of 2° in Figure 19 for the R/f = 0.7 lens with the 2° curve in Figure 20 for R/f = 0.6.

A reduction in the peak position shift with increasing curvature is portrayed in Figure 21 where the peak shifts for an f/1.0 flat and an R/f = 0.7 lens are compared. This reduction also is responsible for the improvement in tracking error sensitivity.

Figure 22 shows interesting changes in the peak concentration ratios observed as a function of transverse deviation. As in previous studies [2-5], for a flat lens the peak concentration ratio initially increases slightly for small tracking errors and then decreases substantially for
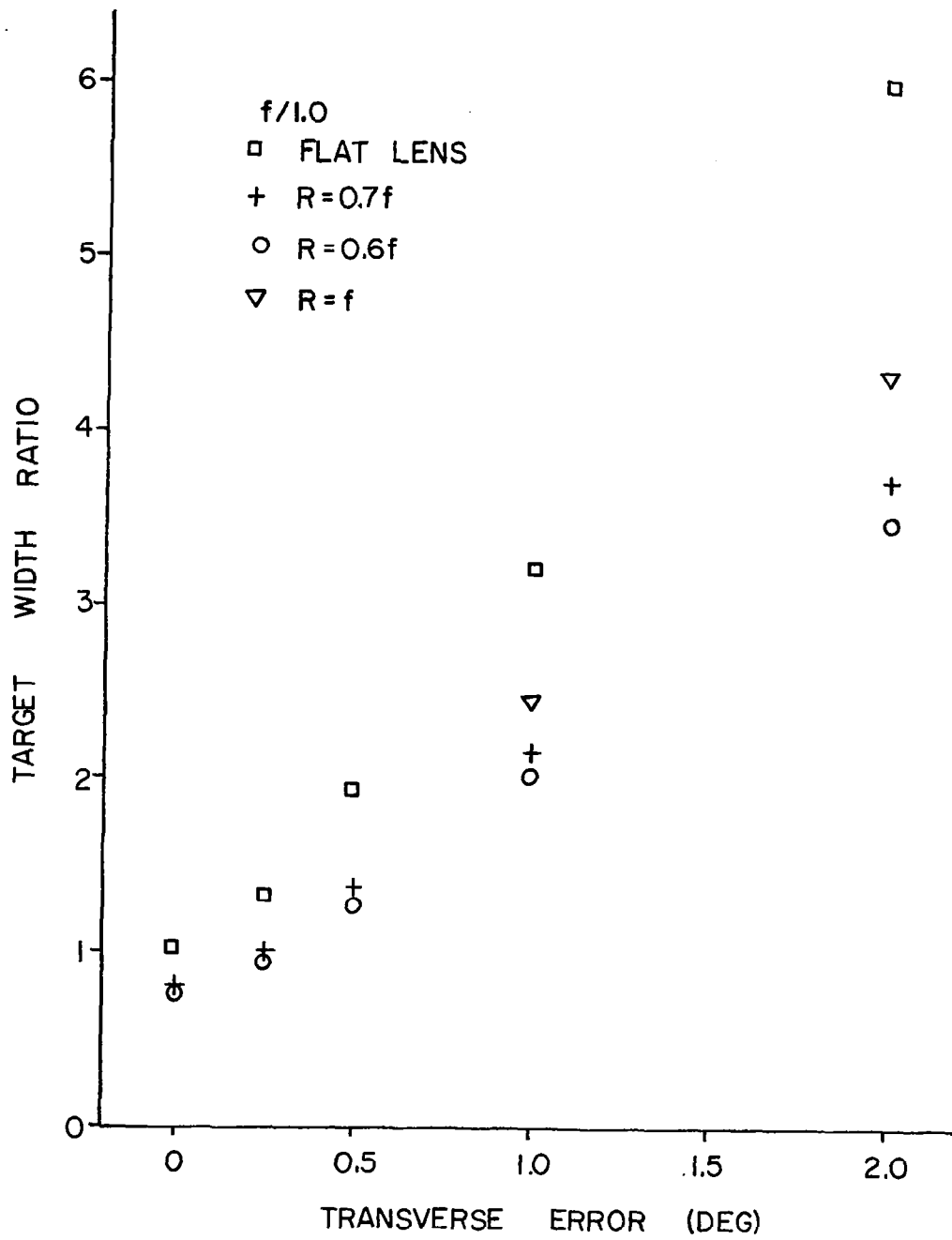
Figure 16. Transverse orientation effects on
target width for an f/1.0 lens.
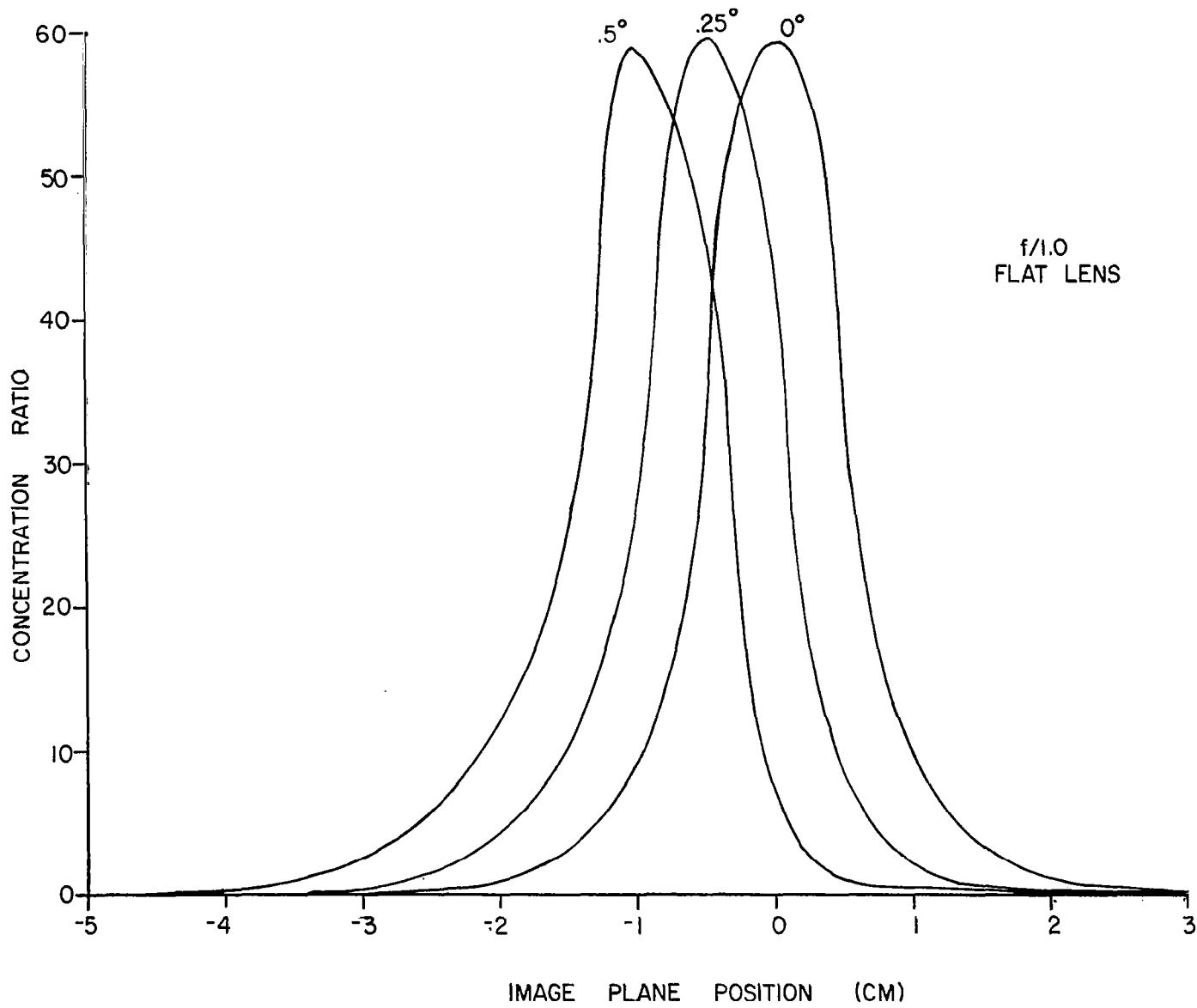
Figure 17.   Transverse orientation effects on image profile for an f/1.0 flat lens.
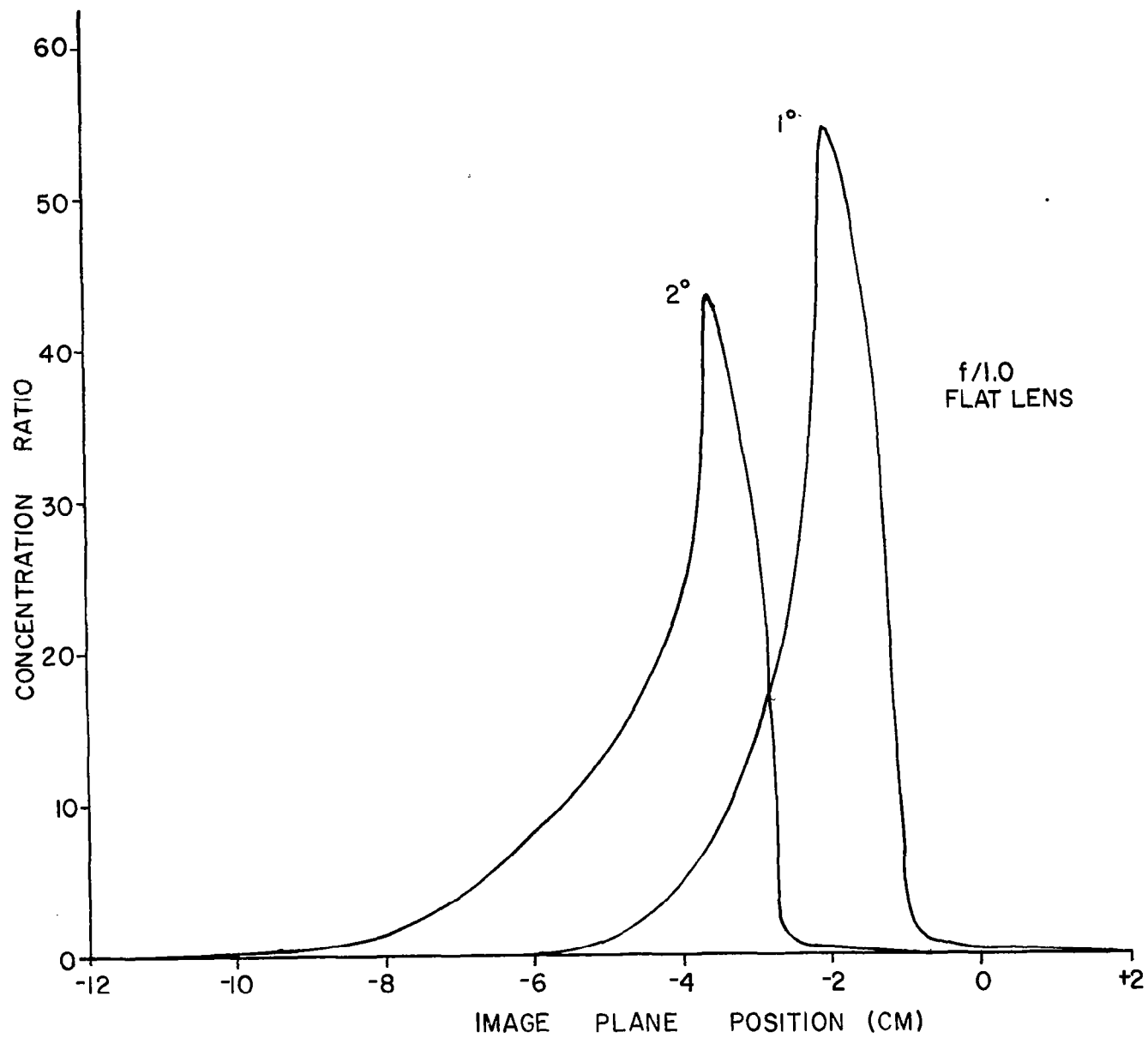
Figure 18. Transverse orientation effects on image profile for an f/1.0 flat lens.
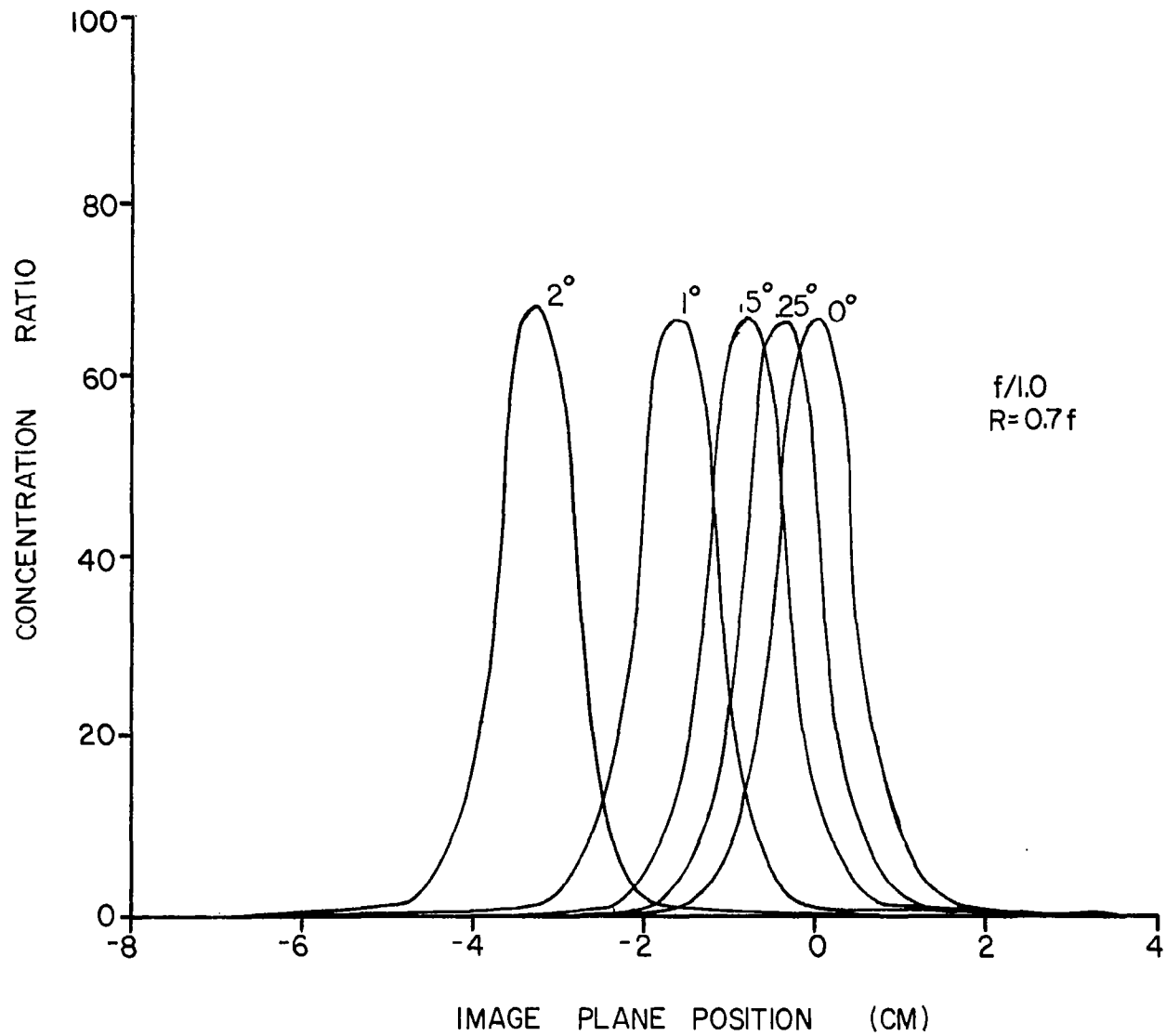
Figure 19.   Transverse orientation effects on image profile for a curved f/1.0 lens..
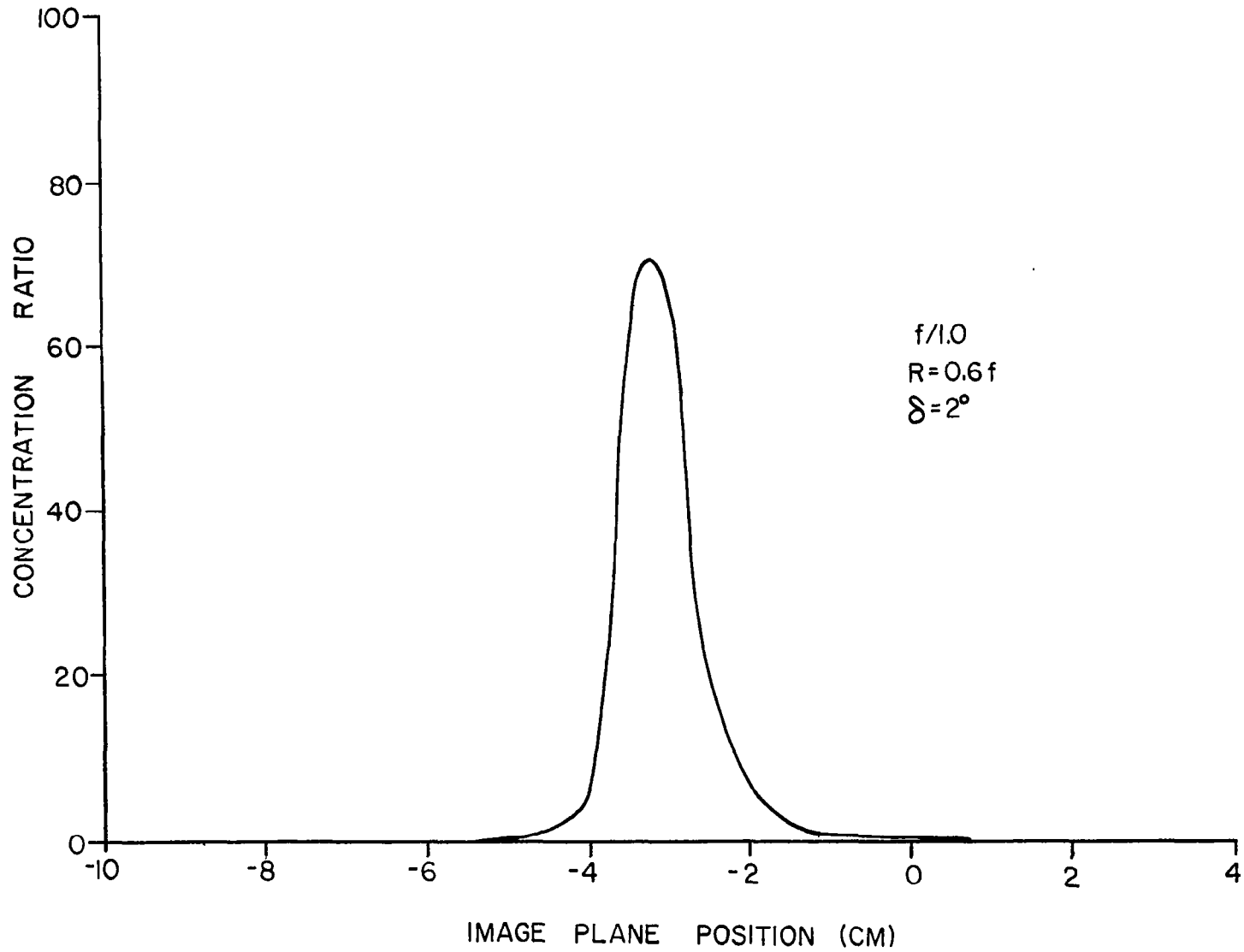
Figure 20. Image profile for 2° tracking misalignment for a curved f/1.0 lens.
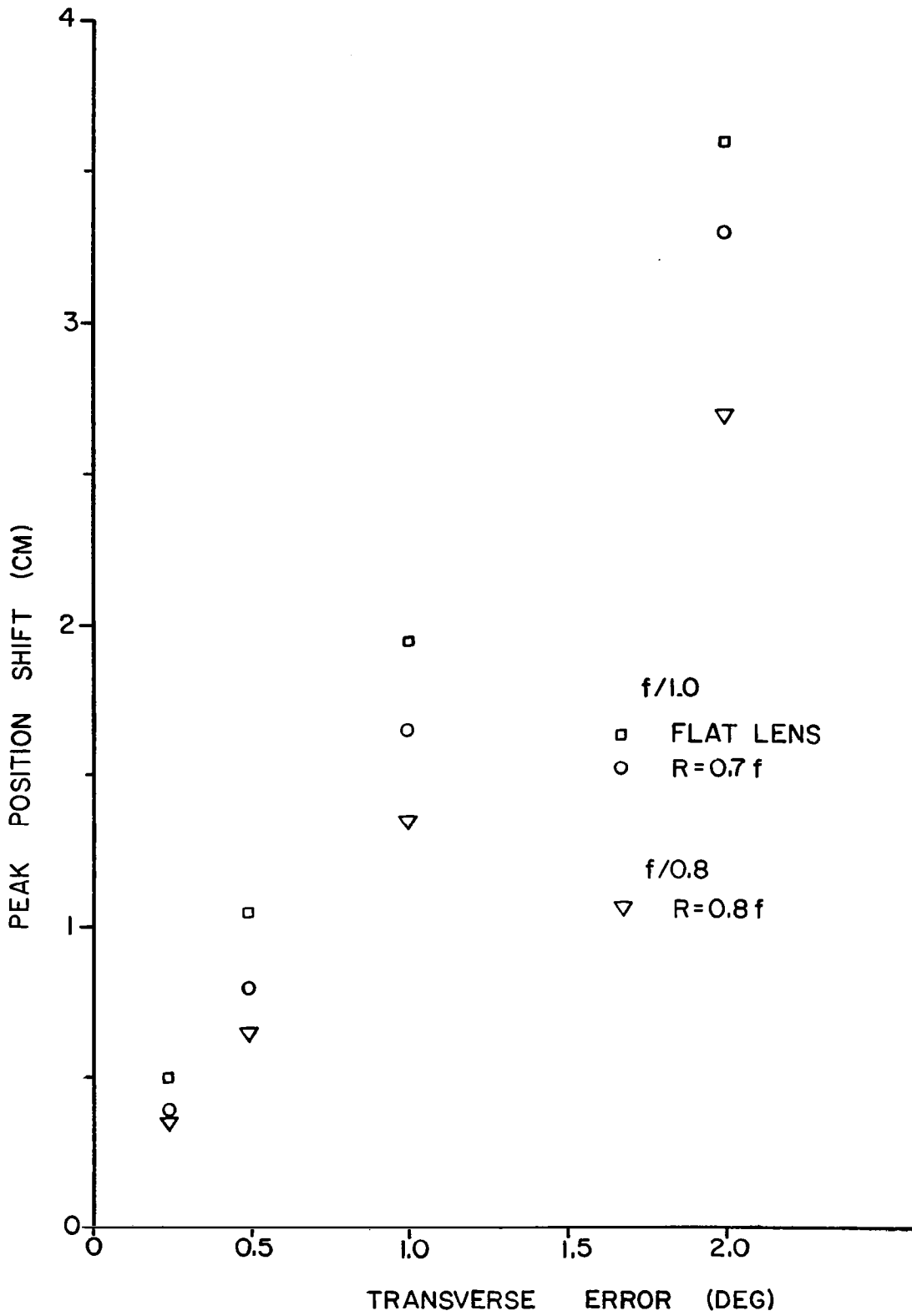
Figure 21. Transverse orientation effects on profile position.
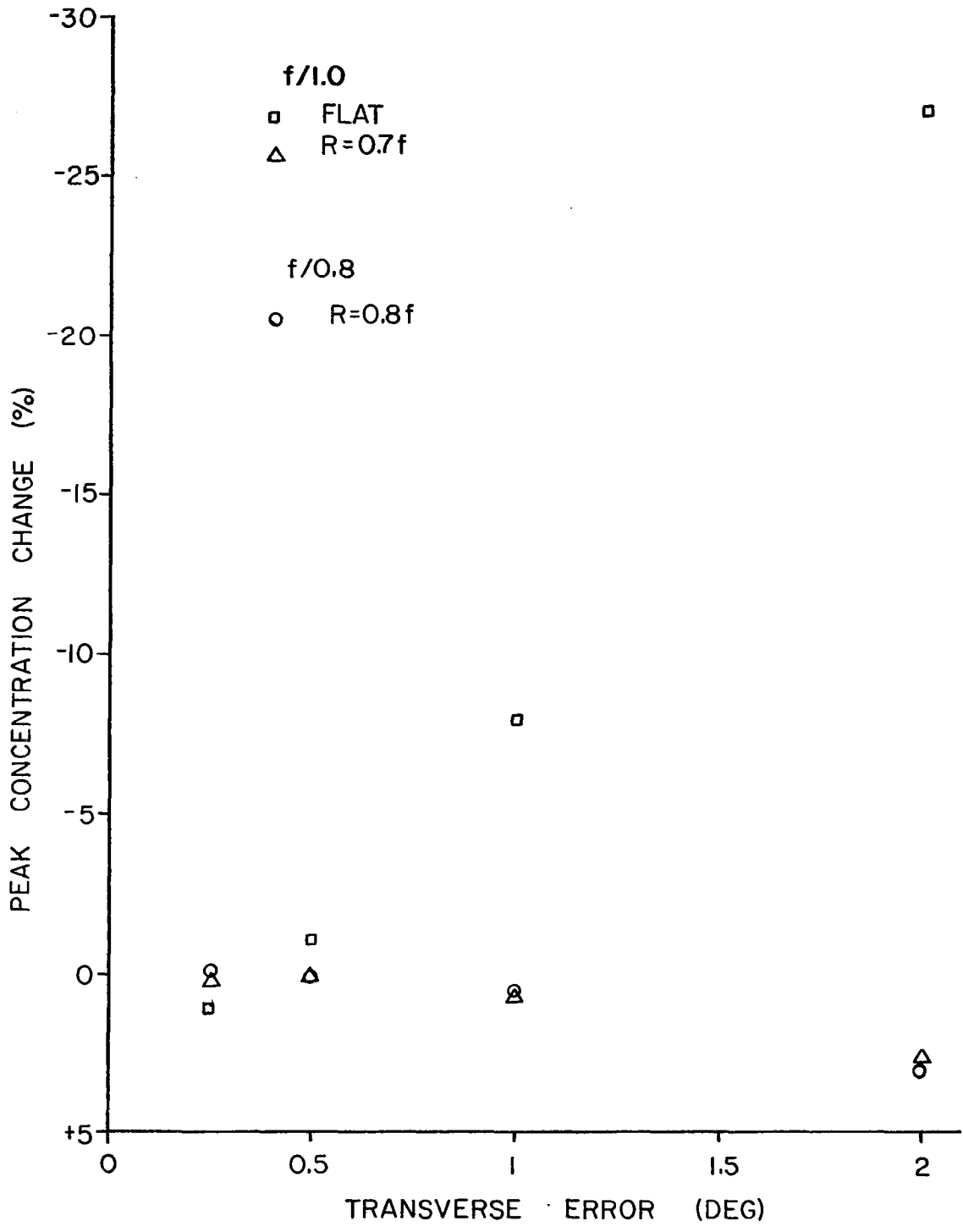
Figure 22. Transverse orientation effects on peak concentration.

errors of 1° or more. For the curved lens data, the peak concentration ratio increases by small percentages over the entire 0°-2° range of tracking deviations studied. Since slight profile asymmetry begins to appear at the upper end of this range and increases as the curvature increases, a decrease in peak concentration ratios is suggested for larger tracking errors and/or smaller curvature radii. Thus it would seem the flat lens peak concentration behavior with tracking deviation probably occurs for much larger errors for curved lenses.

For other f-number lenses, the tracking sensitivities and conclusions with respect to base curvature are similar to that discussed above for the f/1.0 lens. Figure 23 illustrates the target width dependence on transverse error for an f/0.8 lens and three different curvatures. The image profiles for an f/0.8, R = 0.8f lens with tracking errors 0°-2° are depicted in Figure 24. Peak position shift and peak concentration ratio changes are recorded in Figures 21 and 22.

With the current analytical model and associated computer program, detailed studies of the serration and spectral contributions to the image profiles are possible. The influence of dispersion can be examined by, e.g., studying the extreme ray intercepts in the focal plane for various spectral components. In Figure 25 (a), (b), and (c), the intercept results for refraction of solar wavelengths in the ultraviolet, visible, and infrared parts of the solar spectrum by serrations on an f/0.8, R/f = 0.8 lens concentrator with a 2° transverse tracking error are illustrated. These extreme ray intercepts may be compared with those for an identical, perfectly tracking lens (Figure 26 (a), (b), (c)). For the zero tracking error case and serrations near the lens optic axis, the ray intercepts are symmetrical about the zero position in the focal plane.

43
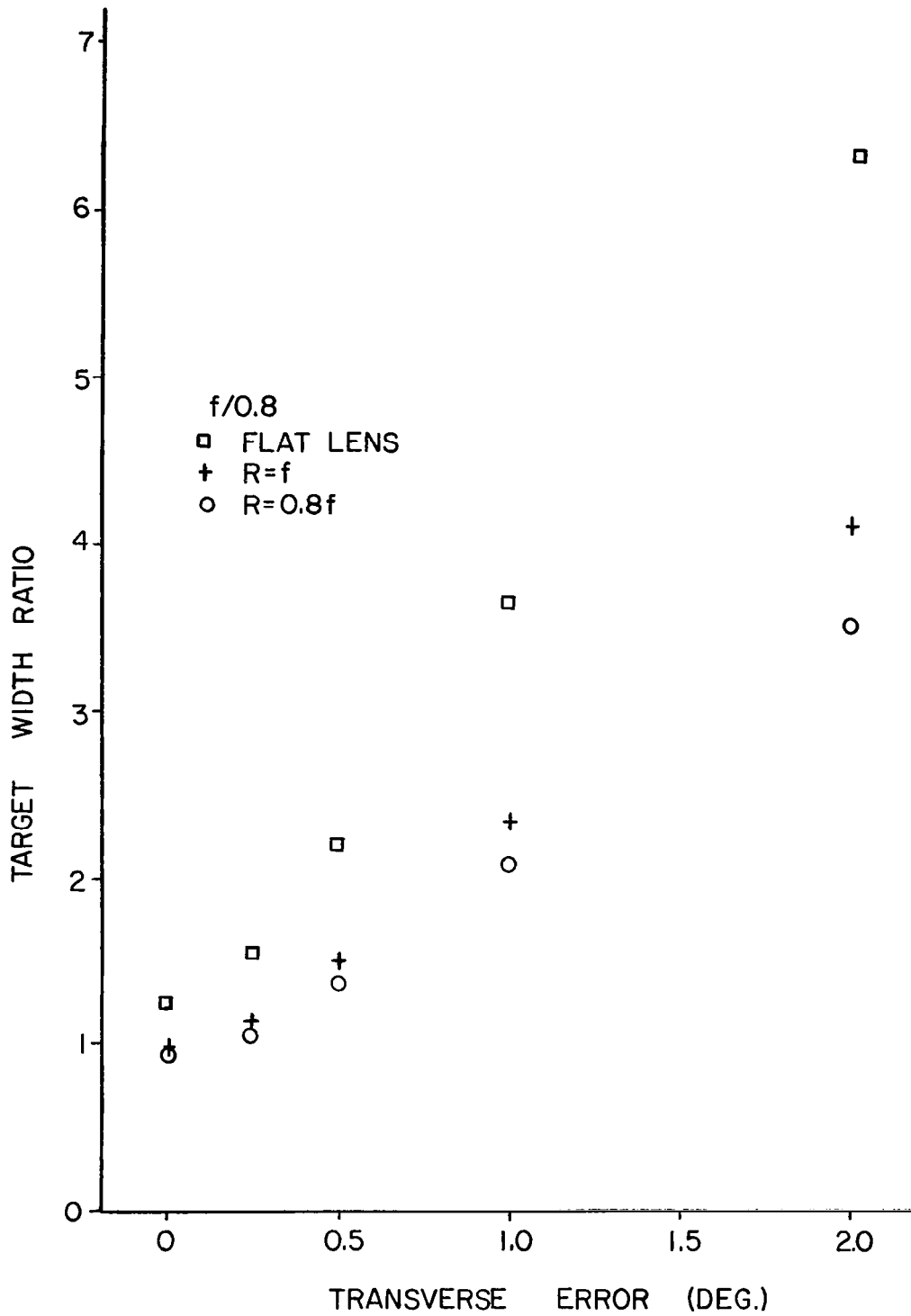
Figure 23. Transverse orientation effects on target width for an f/0.8 lens.
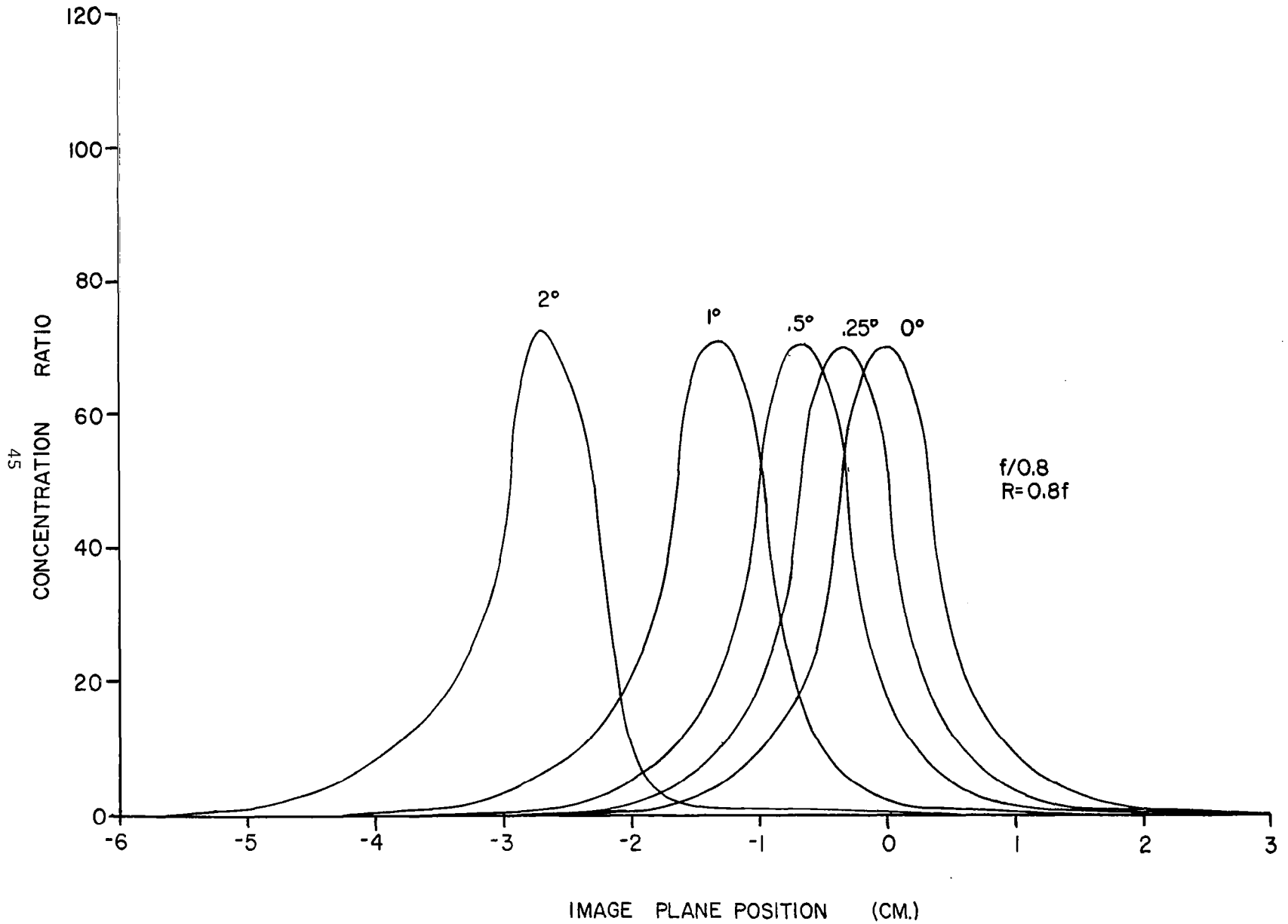
Figure 24. Transverse orientation effects on image profile for a curved f/0.8 lens.
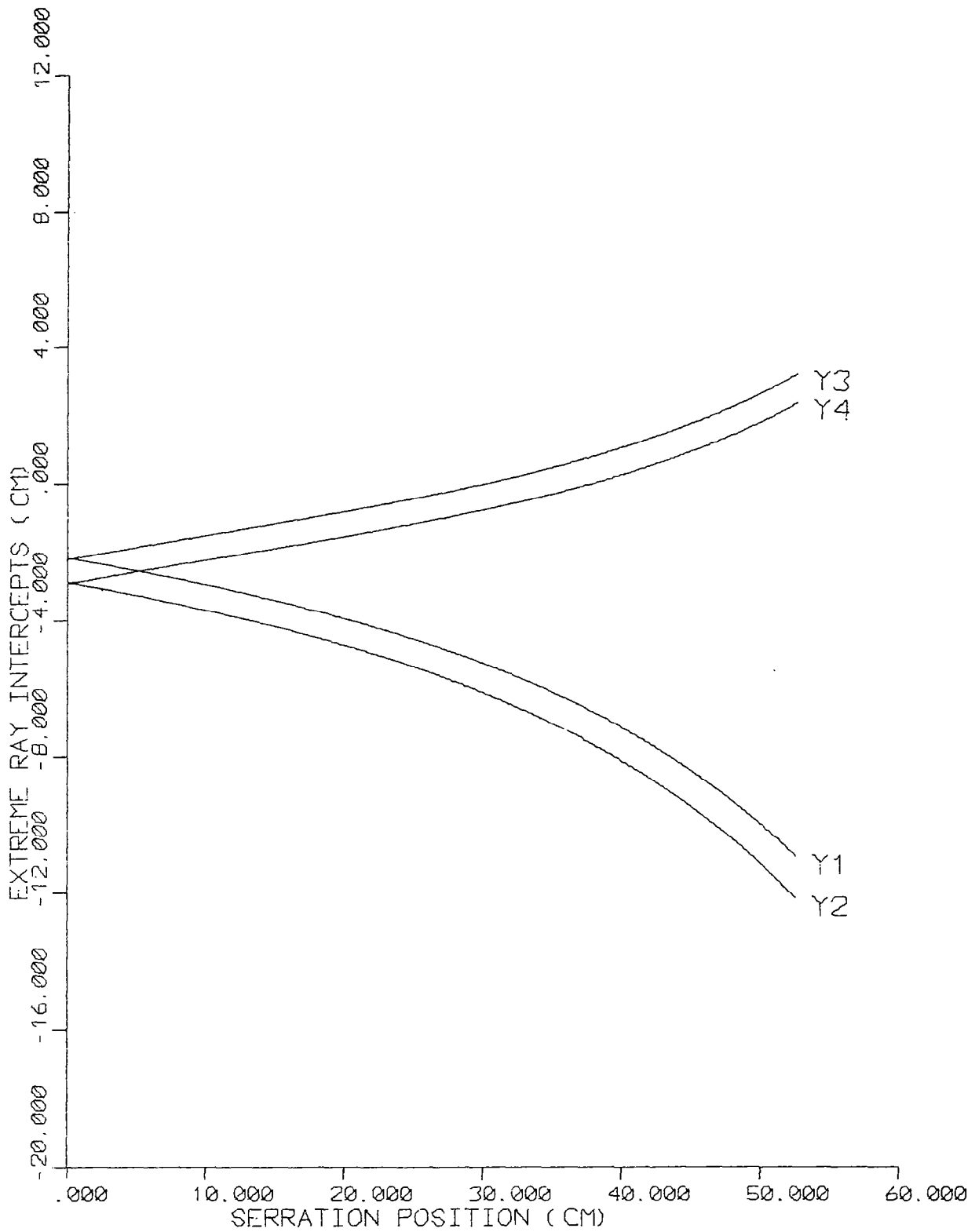
(a)

Figure 25. Extreme ray intercepts for an f/0.8 curved lens with 2° tracking error. Solar wavelengths: (a) 3740 Å (UV) (b) 6150 Å (c) 16400 Å (IR).

(b)

Figure 25.

47

(c)
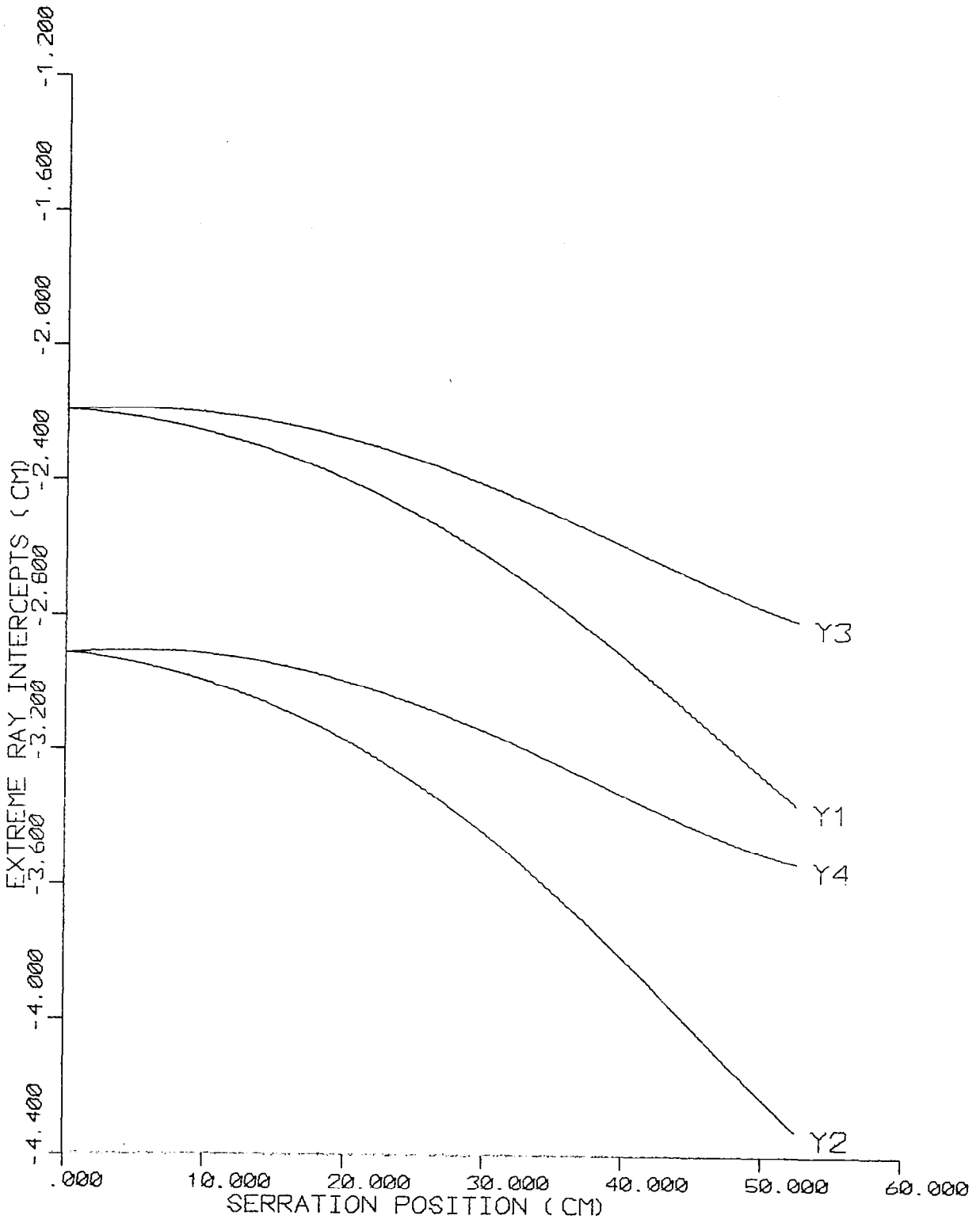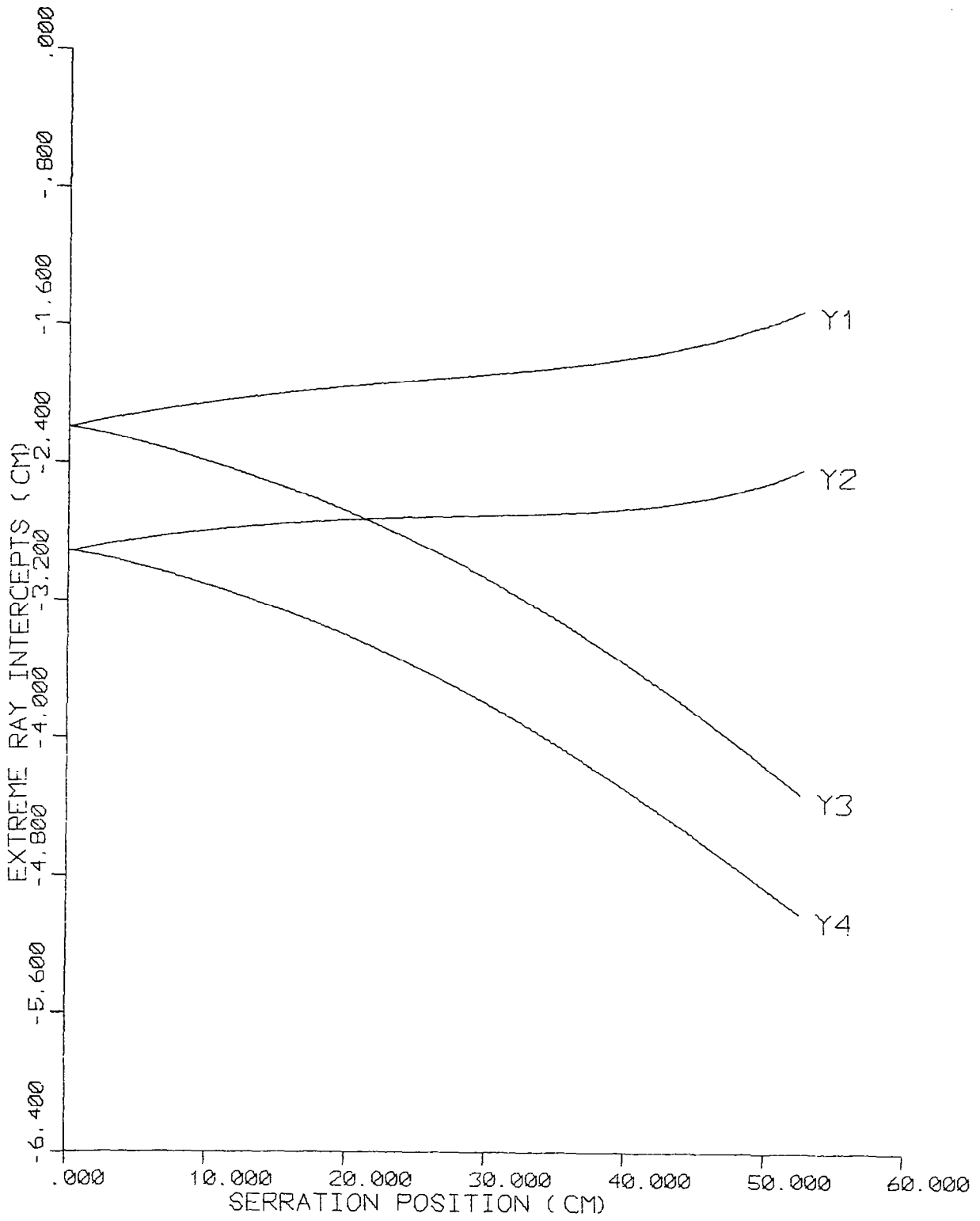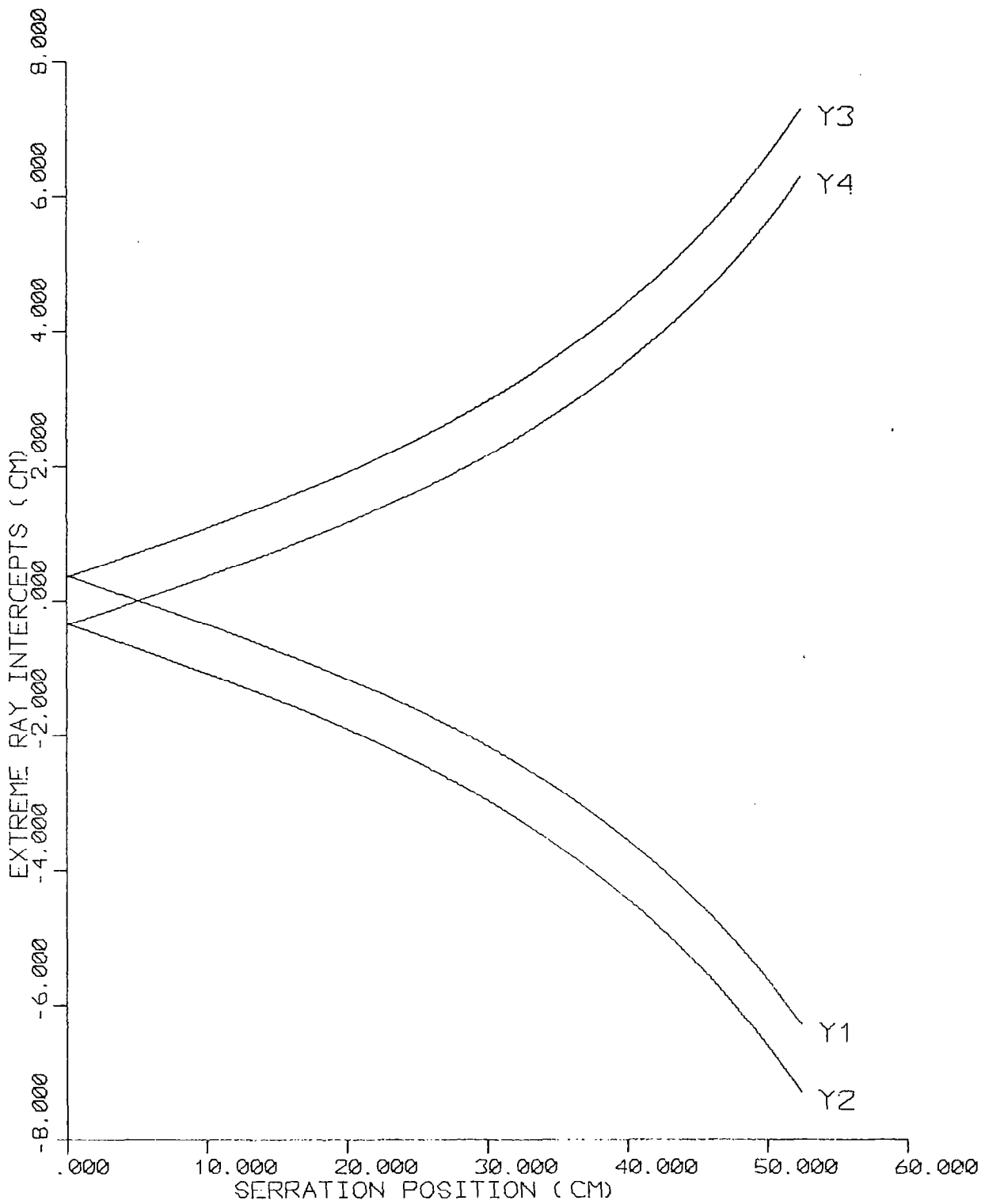
Figure 25.

Figure 26. Extreme ray intercepts for a perfectly tracking f/0.8 curved lens. Solar wavelengths: (a) 3740 Å (UV) (b) 6150 Å (c) 16400 Å (IR).

49

(b)

Figure 26.

50

(c)

Figure 26.

51
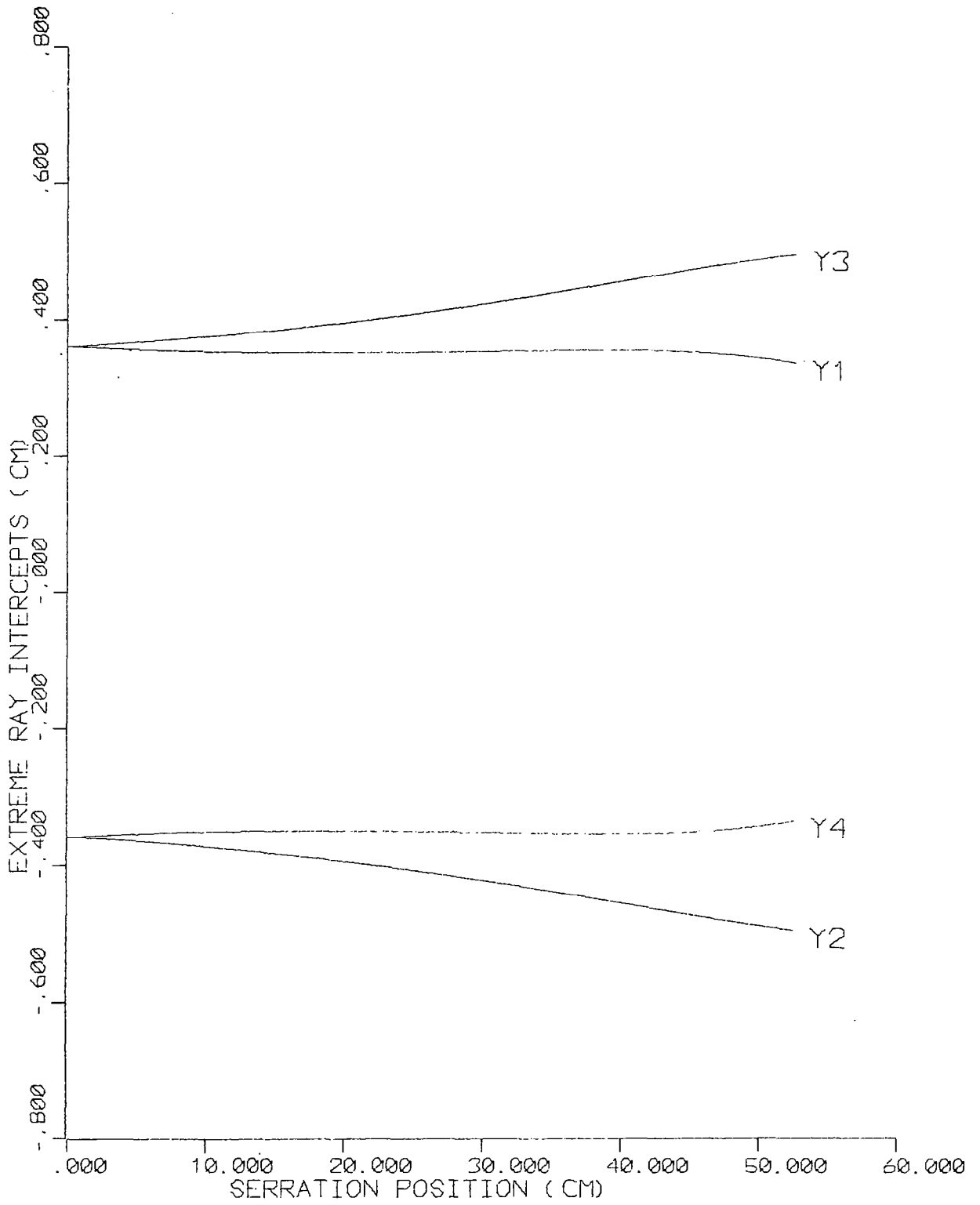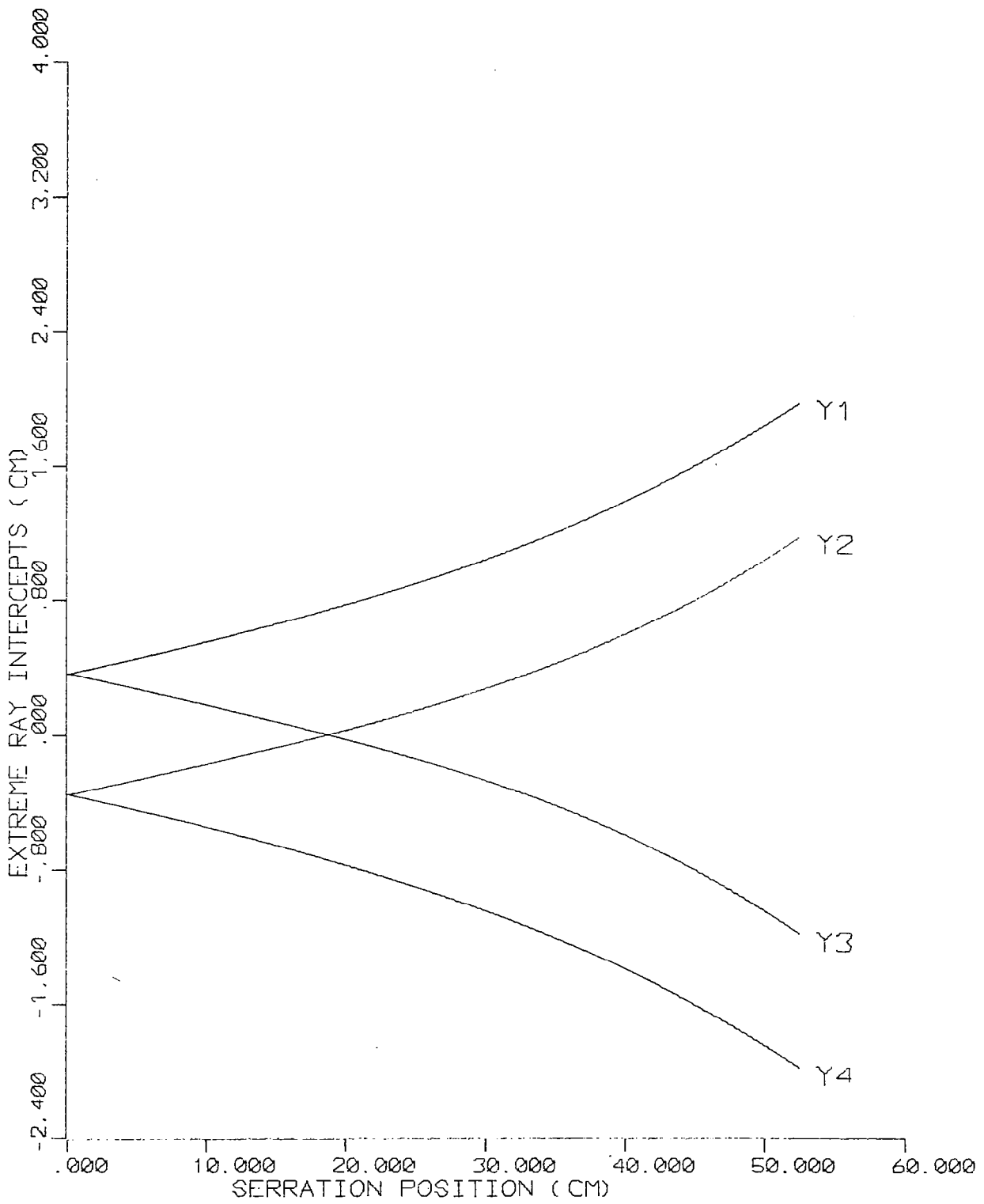
Excessive ray refraction in the UV region contrasts with insufficient IR redirection. For wavelengths near the design wavelength, lens focusing is obviously good. For 2° transverse deviation, the intercepts exhibit a similar wavelength dependence, but are grossly shifted in the negative direction.

3. Defocusing Performance

To ascertain the effects of small errors in locating the target receptor at the lens design focal plane, image intensity profiles for defocusing percentages in the range +2% to -2% of the focal length were studied for perfectly tracking lenses with various f-numbers and curvatures. Target width results are displayed in Figures 27 and 28 for f/1.0 and f/0.8 lenses. Close inspection of the data shows that the rate of increase of the target width with defocusing is highest for lenses with the most curvature. Thus, compared with the defocusing characteristics of a flat lens, the curved lens concentrator performance is more sensitive to small displacements of the target receptor from the intended image plane. For an f/0.8, R/f = 0.8 lens, the required target width increases by 27% when the selected image plane is shifted 1% closer to the lens than the focal plane, as compared to 13% for a flat lens with the same f-number.

As reported earlier for flat lenses [4], the minimum in the target width dependence on defocusing does not occur at the focal plane for the selected lens design index of refraction of 1.49. For the lens cases investigated in this study, the optimum target location occurs at approximately the +0.5% "defocused" image plane. Optimization of the design wavelength would, it is speculated, shift the minimum target width image plane to the focal plane. The slight effects of the thin lens
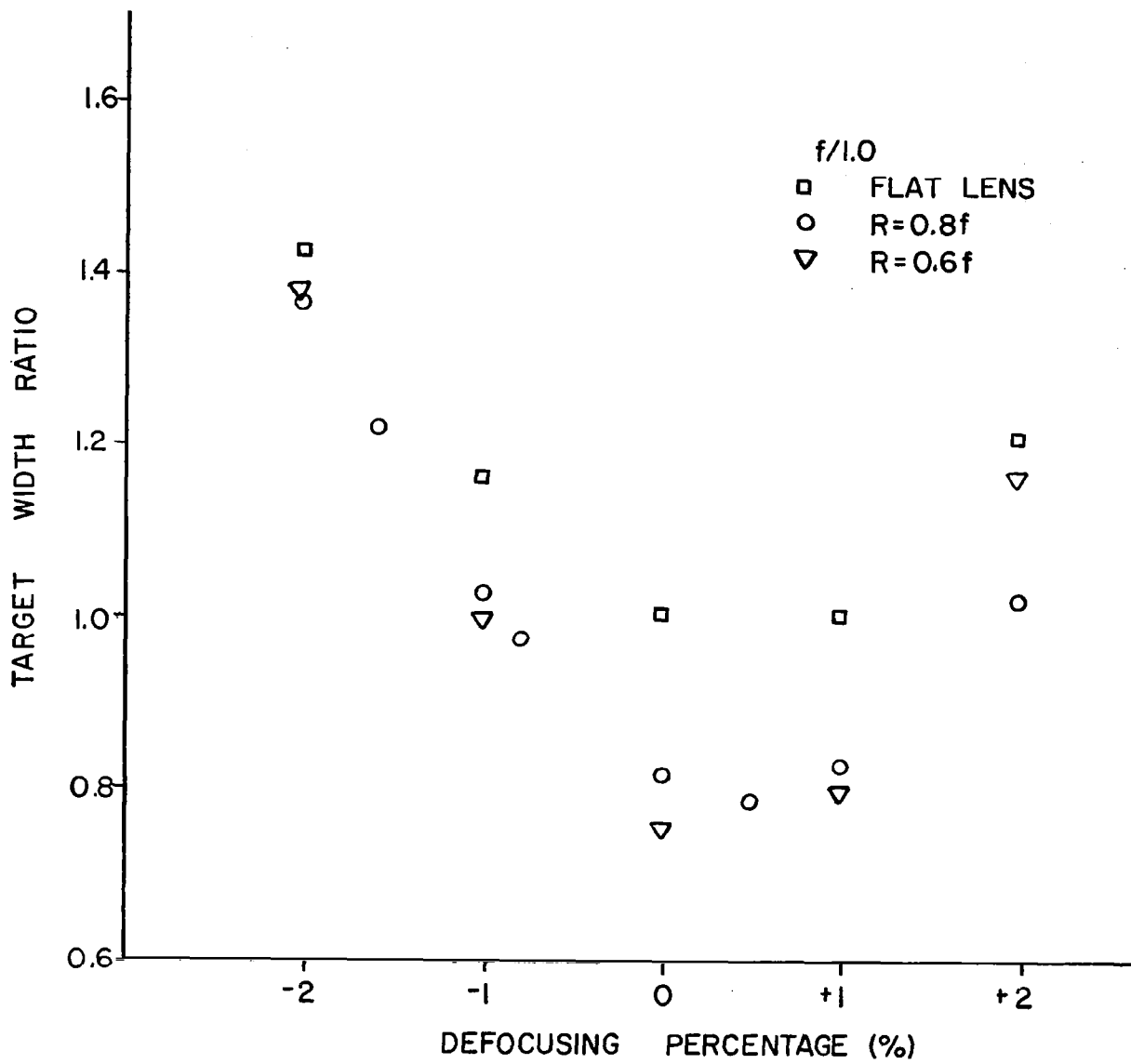
Figure 27. Target width variation with defocusing for f/1.0 lenses.
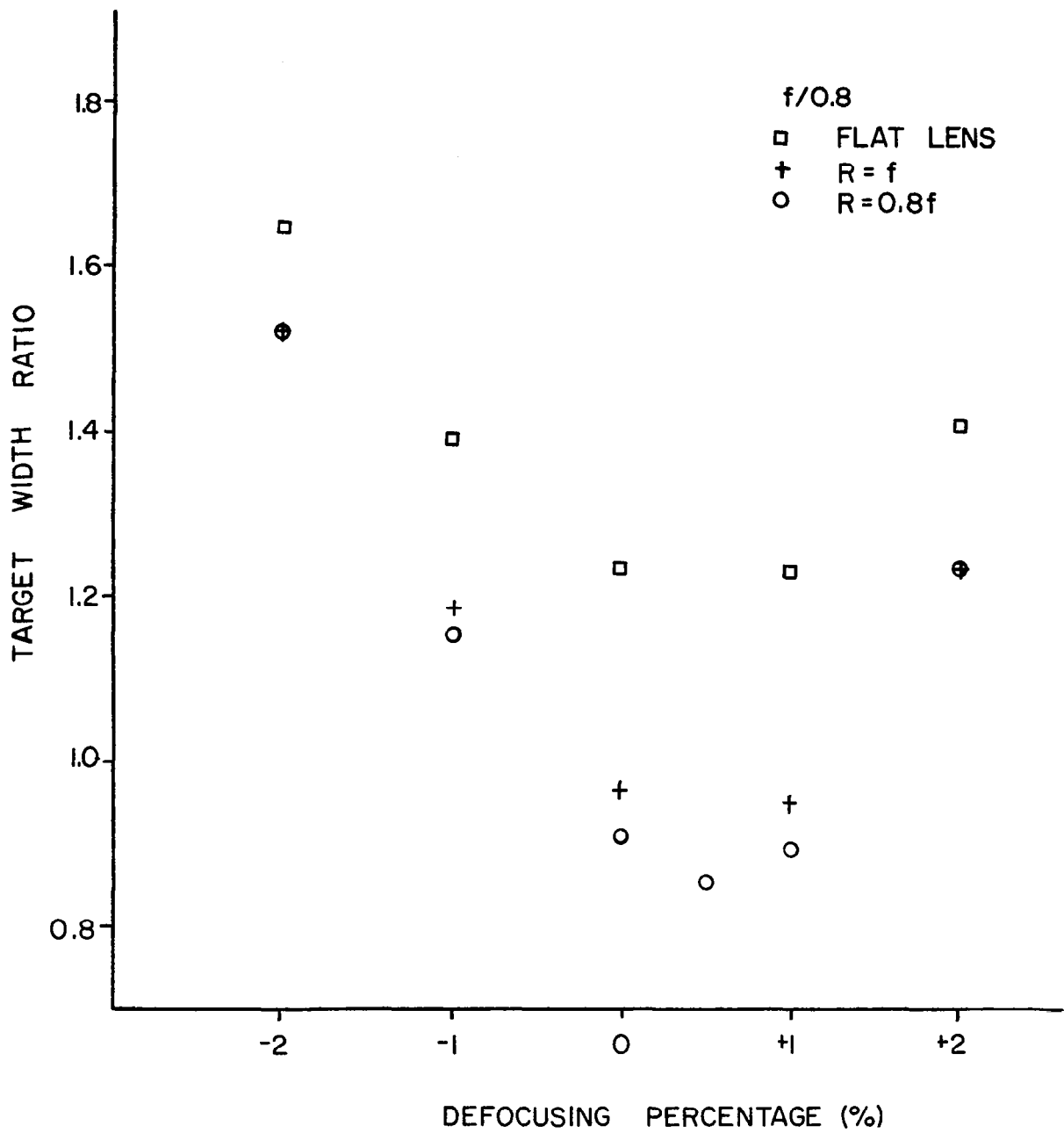
Figure 28. Target width variation with defocusing for f/0.8 lenses.

approximation in determining groove angles may also have a very small influence on the non-focal plane location of the minimum target width.

Comparing the intensity profiles in Figures 29 and 30 for an f/0.8, R/f = 0.8 lens, defocusing generally broadens the profile and lowers the concentration ratio, substantially so for image planes 2 to 2½% from the minimum target width plane.

For the 0.5% defocused position (minimal target width plane), the sensitivity to tracking error was investigated for an f/0.8, R/f = 0.8 lens. Lens performance was very similar to that in Figure 23 for the focal plane case, with target widths slightly reduced for all deviations (0°-2°) examined.

IV. CONCLUSIONS

Curving the base of a grooves down, line-focusing Fresnel lens significantly improves overall lens solar concentration performance. Model results indicate:

- Required target receptor widths generally decrease with increasing curvature; peak concentration values increase (>70 for some cases).

- Lens solar transmission is high, generally in the range 85-88%, increasing slightly as the curvature is enhanced over the flat lens case and then decreasing for the lowest curvature radii.

- Performance sensitivity to small (≤2°) transverse tracking errors can be significantly less for curved lenses as compared to flat lens tracking sensitivity:

    -Required focal plane target widths increase with tracking error at a lower rate for curved base lenses.

    -Profile asymmetry is drastically reduced.

    -Profile shift for a given tracking deviation is less.

    -In contrast to the dominant behavior for the flat lens, peak concentration values increase over the 2° range investigated.

    -As in the flat lens case, lens transmission is essentially unaffected.
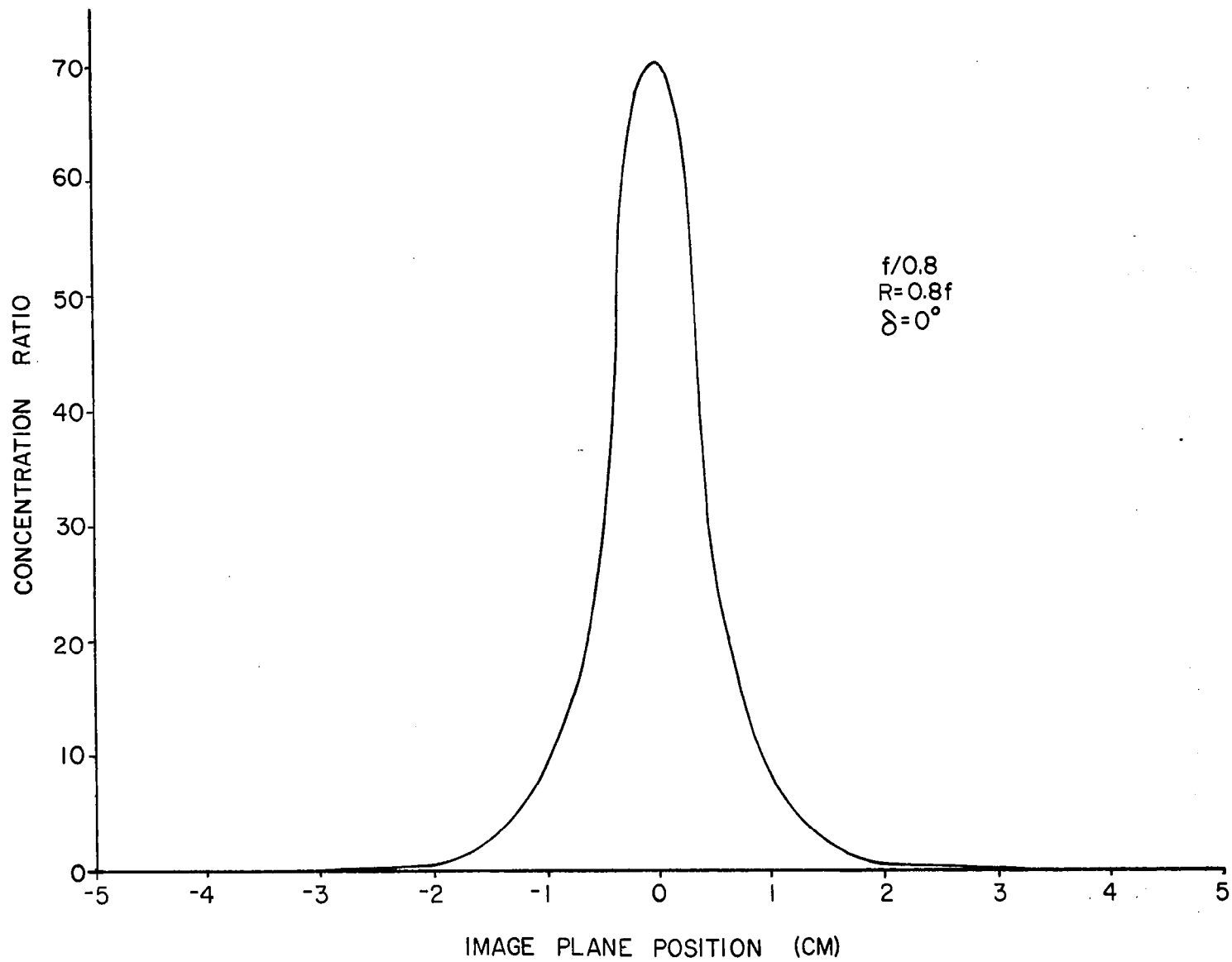
Figure 29.   Focal plane image profile for a curved lens.

70 —

60 —

50 —

40 —

30 —

20 —

10 —

0 —

CONCENTRATION RATIO

% Defocused

+1

+2

-2

f/0.8
R= 0.8f
δ = 0°

-5   -4   -3   -2   -1   0   1   2   3   4   5

IMAGE PLANE POSITION   (CM)
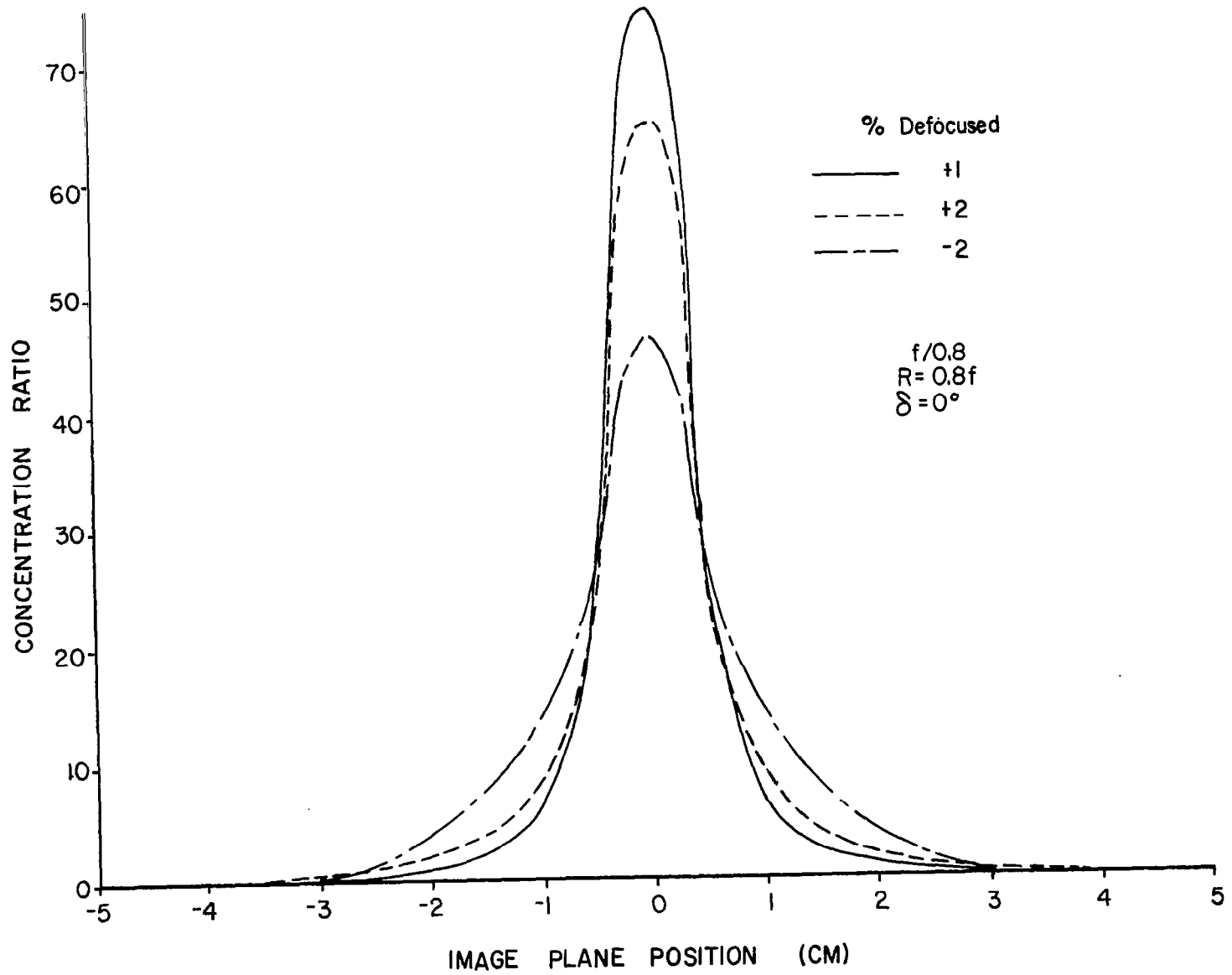
Figure 30.   Defocused intensity profiles above (-) and below (+) the focal plane.

- Solar image profile characteristics are substantially more sensitive to slight defocusing than for the flat lens case. Thus placement of a target receptor beneath a curved lens concentrator must be done accurately in order to take advantage of the improvements in concentration performance. This is the primary negative effect of curvature on lens performance.

    -The target width minimum and peak concentration ratio occur at a slightly defocused position for the lens design parameters chosen.

    -Defocusing relative to the above minimum position broadens the intensity profile and decreases the peak concentration ratio.

    -Required target widths increase with defocusing at a higher rate for curved lenses than for flat lenses.

- The optimum curvature radius for an f/0.7 lens occurs at approximately $R = 0.8f$. For larger f-numbers, the optimum radius is evidently near the minimum radius for the ideal lenses analyzed. This optimum radius is suggested to be sensitive to small lens transmission changes.

Compared to an f/1.0 flat lens, selection of a curved base Fresnel concentrator with $0.8 \leq$ f-number <1.0 and curvature radius $R \leq f$ is predicted to improve the solar optical performance while decreasing structural size and tracking mechanism requirements.

V. REFERENCES

1. L. Hastings, S. Allums, and W. Jensen, "An Analytical and Experimental Investigation of a 1.8 By 3.7 Meter Fresnel Lens Solar Concentrator", ISES-Amer. Sec. Conf. Proc., Orlando, FL, (6-10 June 1977), to be published.

2. L. Hastings, S. Allums, and W. Jensen, "An Analytical and Experimental Investigation of a 1.8 By 3.7 Meter Fresnel Lens Solar Concentrator", NASA Technical Memorandum, to be published, 1977.

3. R. Cosby, "The Linear Fresnel Lens: Solar Optical Analysis of Tracking Error Effects", ISES-Amer. Sec. Conf. Proc., Orlando, FL, (6-10 June 1977), to be published.

4. L. Hastings, S. Allums, and R. Cosby, "An Analytical and Experimental Evaluation of a Fresnel Lens Solar Concentrator", NASA TM X-73333, August, 1976.

5. L. Hastings, S. Allums, and R. Cosby, "An Analytical and Experimental Evaluation of the Plano-Cylindrical Fresnel Lens Solar Concentrator", ISES Conf. Proc., Winnepeg, Manitoba, Canada, Vol. 2 (15-20 August 1976).

6. P. Moon, "Proposed Standard Solar-Radiation Curves for Engineering Use", J. Franklin Institute, 23a, 583 (1940).

7. Rohm and Haas Company, Philadelphia, PA, "Plexiglas Injection and Extrusion Molding Powders", Publication PL 165f, (1968).